Quaternary Science Reviews
December 2023, Volume 322 Pages 108431 (13p.)
https://doi.org/10.1016/j.quascirev.2023.108431
https://archimer.ifremer.fr/doc/00861/97311/

Long-term variability of the western tropical Atlantic sea surface temperature driven by greenhouse gases and AMOC

Nascimento R.A. [1,*], Johnstone H.J.H. [2], Kuhnert H. [2], Santos T.P. [1], Venancio I.M. [3], Chiessi C.M. [4], Ballalai Joao Marcelo [3,5], Campos M.C. [6,7], Govin A. [8], Mulitza S. [2], Albuquerque A.L.S. [1]

[1] Departamento de Geologia e Geofísica, Universidade Federal Fluminense, Niterói, Brazil
[2] MARUM - Center for Marine Environmental Sciences, University of Bremen, Bremen, Germany
[3] Programa de Geociências (Geoquímica), Universidade Federal Fluminense, Niterói, Brazil
[4] School of Arts, Sciences and Humanities, University of São Paulo, São Paulo, Brazil
[5] UMR 6538 Geo-Ocean, CNRS, IFREMER, UBO, UBS, Centre de Bretagne 29280 Plouzané, France
[6] Institute of Geosciences, University of São Paulo, São Paulo, Brazil
[7] Institute of Geosciences, University of Campinas, Campinas, Brazil
[8] Laboratoire des Sciences Du Climat et de L'Environnement/Institut Pierre Simon Laplace, CEA-CNRS-UVSQ, Université Paris Saclay, Gif sur Yvette, France

* Corresponding author : R. A. Nascimento, email address : rodrigoan@id.uff.br

Abstract :

The long-term orbital-scale sea surface temperature (SST) variability in the tropics is thought to be mainly driven by greenhouse gases (GHG) forcing. However, few studies have investigated the drivers of such variability in the tropical Atlantic. Given the evidence of orbital-scale changes in Atlantic Meridional Overturning Circulation (AMOC) strength, one can hypothesize that AMOC variability also modulates the long-term tropical Atlantic SST through the bipolar seesaw mechanism. According to this mechanism, under weak [strong] AMOC conditions, the Southern Hemisphere is expected to warm up [cool down], while the Northern Hemisphere cools down [warms up]. Here, we investigate the long-term SST variability of the western tropical South Atlantic (WTSA), i.e., along the main pathway of the upper AMOC branch towards the equator, using a new 300 thousand years (kyr)-long Mg/Ca-based SST record. Our SST record shows glacial-interglacial variability superimposed by four remarkable long-term warm events during the three recorded glacial periods. These glacial warm events occurred between ca. 280–260, 160–143, 75–60, and 40–24 ka before present. Our results support the notion that atmospheric GHG plays a leading role in modulating the glacial-interglacial SST variability in the WTSA. However, it does not explain the occurrence of glacial warm events. Our study supports that the glacial warm events were caused by an orbital-scale bipolar seesaw mechanism operating in the Atlantic due to changes in the AMOC strength. These warm events may have been amplified by annual mean insolation driven by obliquity. Finally, we suggest that the long-term bipolar seesaw warmed the western tropical (South) Atlantic during the MIS 5/4 transition when the Earth's climate was cooling off.

Highlights

► The western tropical South Atlantic SST was reconstructed for the last 300 kyr. ► Greenhouse gases control the glacial-interglacial SST variability. ► Four long-term warm events were identified during glacial conditions. ► The warm events were caused by an orbital-scale bipolar seesaw in the Atlantic.

Keywords : Sea surface temperature, Western tropical Atlantic, Glacial cycles, Orbital-scale, Bipolar seesaw

1. Introduction

Ice core records show a remarkable resemblance between atmospheric CO_2 concentration and glacial-interglacial cycles in Antarctic temperature over the last 800 thousand years (kyr) (Lüthi et al., 2008). This linkage is attributed to the fact that changes in atmospheric CO_2 concentration, more broadly greenhouse gas (GHG), alter radiative forcing, thereby modulating the Earth's climate on orbital-scale (Barnola et al., 1987; Genthon et al., 1987; Shakun et al., 2012). As tropical latitudes are far from the direct influence of high-latitude continental ice sheets, they are ideal for investigating the equilibrium response of the sea surface temperature (SST) to long-term changes in GHG concentrations (Broccoli, 2000). Although the annual mean SST in the tropics can also be modulated by insolation forcing (Berger et al., 2010; Loutre et al., 2004; Timmermann et al., 2007), studies from the tropical Pacific support the notion that the long-term SST variability is mainly controlled by glacial-interglacial changes in GHG concentration (Dyez and Ravelo, 2013; Lea, 2004). In particular, a transient model simulation suggests that only 18% of SST variability in the western tropical Pacific is forced by non-CO_2 effects (Tachikawa et al., 2014).

Unlike the Pacific Ocean, the SST in the tropical Atlantic is strongly affected by the strength of the Atlantic Meridional Overturning Circulation (AMOC), which is responsible for the net cross-equatorial northward heat transport in the Atlantic Ocean. Currently, the AMOC transports ca. 0.4 Peta Watts (0.4 x 10^{15} Watts) across the equator (Marshall et al., 2014) along the upper western tropical Atlantic margin, the main pathway for this cross-equatorial heat transport (Zhang et al., 2011). The subsequent heat loss to the atmosphere at high latitudes of the North Atlantic prompts deep convection and the formation of the North Atlantic Deep Water (NADW) that flows southward in the deep ocean (Srokosz et al., 2012). The Atlantic SST responds to variations in the AMOC via the so-called thermal bipolar seesaw mechanism (Stocker and Johnsen, 2003). When the AMOC is weak, the Southern Hemisphere is expected to warm up while the Northern Hemisphere cools down; the opposite should occur when the AMOC is strong (Pedro et al., 2018). Therefore, the weakening of the northward cross-equatorial heat transport during the AMOC slowdown is expected to warm up the western tropical Atlantic (Crowley, 1992; Mix et al., 1986). Instrumental observations, model simulations, and proxy-based reconstructions have corroborated the role of the AMOC in modulating the western tropical Atlantic SST from decadal to millennial timescales (Crivellari et al., 2019; Pedro et al., 2018; Rühlemann et al., 1999; Venancio et al., 2020; Yang, 1999; Zhang et al., 2011). However, studies have pointed to oscillations in North Atlantic deep convection and AMOC strength also on long-term orbital-scale (Lisiecki, 2014; Lisiecki et al., 2008). Assuming these long-term variations in AMOC intensity, one might expect these to have affected the western tropical Atlantic SST variability through a sort of orbital-scale bipolar seesaw mechanism (e.g., Lisiecki et al., 2008).

However, the scarcity of long records with appropriate resolution encompassing several glacial cycles hinders understanding the forcings and mechanisms controlling the long-term variability of SST in the western tropical Atlantic region. This study investigates the main drivers of long-term changes in a new 300-kyr-long SST record from the western tropical South Atlantic (WTSA). Our SST record is based on the Mg/Ca ratio of planktonic foraminifera *Globigerinoides ruber* (white) shells from the sediment core GL-1180. Our results corroborate that GHG concentration modulated the glacial-interglacial tropical SST variability. However, orbital-scale changes in the AMOC strength were crucial in driving the superimposed long-term SST variability observed in western tropical (South) Atlantic records.

2. Study area

Our study region is located in the southern portion of the Atlantic warm pool (Fig. 1a). Modern SST in the region is 27.5 °C on average, with a seasonal amplitude of 1.3 °C (Locarnini et al., 2019). The Atlantic warm pool results from the trade wind stress over the tropical Atlantic. The wind stress piles up warm waters on the western side of the tropical Atlantic and prompts upwelling on the eastern side, causing an east-west tilt in the thermocline depth (Hastenrath and Merle, 1987).

The upper ocean circulation of the tropical South Atlantic is marked by the northwestward-flowing South Equatorial Current (SEC). The SEC reaches the Brazilian margin between 10 and 14°S (Rodrigues et al., 2007), where it bifurcates into the southward-flowing Brazil Current (BC) and northward-flowing North Brazil Under Current (NBUC)/North Brazil Current (NBC) (Stramma and England, 1999). This northward flow is responsible for the net interhemispheric heat transport in the Atlantic as part of the upper limb of the AMOC (Lumpkin and Speer, 2007; Zhang et al., 2011). In the high latitudes of the North Atlantic, namely in the Nordic Seas and the Labrador Sea, the loss of buoyancy prompts the sinking of upper ocean waters into the deep ocean to form the southward flowing NADW, which represents the lower limb of the AMOC (Srokosz et al., 2012). Ultimately, a mix between the colder and saltier waters from the Nordic Seas with fresher and warmer waters from the Labrador Sea composes the lower and the upper portions of NADW, respectively.

Seasonal changes in the WTSA upper ocean circulation are linked to the latitudinal migration of the Intertropical Convergence Zone (ITCZ). The ITCZ position, in turn, is controlled by the seasonal asymmetry in the interhemispheric insolation and heat budget (Marshall et al., 2014; Schneider et al., 2014). During austral winter/spring [autumn/summer], the ITCZ position is displaced northward [southward], strengthening [weakening] southeast trade winds and the

SEC (Rodrigues et al., 2007). The increase in SEC transport during austral winter enhances the pile-up of warm waters in the western tropical Atlantic, steepening the east-west tilt of the tropical Atlantic thermocline and boosting the NBC; the opposite occurs during austral summer/autumn. Accordingly, the mixed layer depth at our study site is deeper during the austral winter (ca. 85 m water depth) relative to the summer (ca. 65 m water depth), with an annual average around 70 m (Fig.1b) (Locarnini et al., 2019). Importantly, the latitudinal displacement of fronts does not influence the study region, and there is no evidence pointing to a local upwelling system.

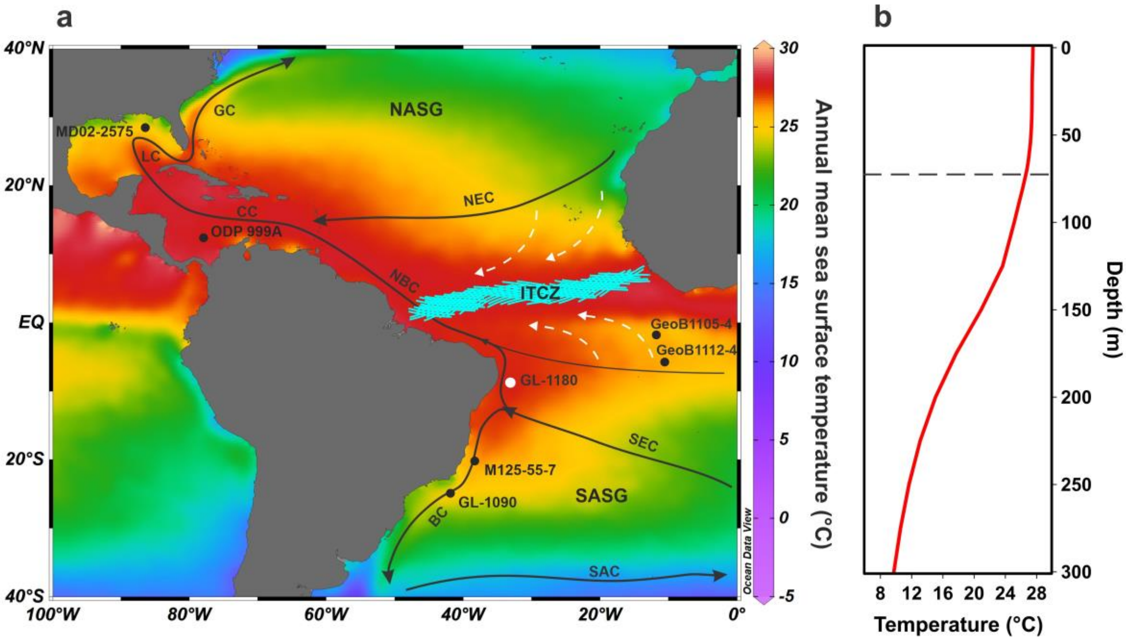

Figure 1: Regional settings of the study region. a) Location of marine sediment core GL-1180 (white dot) and other cores discussed here (black dots): MD02-2575 (Nürnberg et al., 2008; Ziegler et al., 2008); ODP 999A (Schmidt et al., 2006); GeoB1105-4 and GeoB1112-4 (Nürnberg et al., 2000) M125-55-7 (Hou et al., 2020); GL-1090 (Santos et al., 2017). The color scale depicts modern (1955-2017) annual mean sea surface temperatures (Locarnini et al., 2019). Black arrows depict the schematic surface ocean circulation: Brazil Current (BC); Caribbean Current (CC); Gulf Current (GC); Loop Current (LC); North Brazil Current (NBC); North Equatorial Current (NEC); South Atlantic Current (SAC); South Equatorial Current (SEC). NASG and SASG indicate the North and South Atlantic Subtropical Gyres, respectively. The hatched band illustrates the Intertropical Convergence Zone (ITCZ). White dotted arrows show the NE and SE trade winds. The figure was partially generated using the software Ocean Data View (Schlitzer, 2017). b) Annual average vertical temperature profile near the region of sediment core GL-1180 (Locarnini et al., 2019). The dotted line indicates the annual average mixed layer depth (MLD) based on the definition of Kara et al. (2000).

3. Methodology

3.1. Sediment core GL-1180

We investigated marine sediment core GL-1180 (Fig. 1), retrieved by the Brazilian oil company Petrobras at the northeastern continental margin of Brazil (8° 27'18" S, 33° 32'53" W, 1037 m water depth, 1732 cm-long). The sedimentological description of the core does not indicate any sedimentation disturbance, and previous studies have demonstrated the suitability of this sediment core for paleoceanographic and paleoclimatic studies (Nascimento et al., 2021a, 2021b). Sediment samples of approximately 10 cm^3 were taken every 2 cm throughout the core. All sediment samples were wet-sieved to retain a fraction larger than 63 µm. The retained material was dried at 50 °C for 24 hours and stored in acrylic flasks for the geochemical analyses described below.

3.2. Age model

The original age model of sediment core GL-1180 is described in Nascimento et al.(2021b). In brief, the age model was based on six radiocarbon ages measured in shells of planktonic foraminifera (*Globiderinoides ruber* and *Trilobatus sacculifer*) and the visual alignment of the benthic stable oxygen isotopes ($\delta^{18}O$) record of *Cibicides* sp. from sediment core GL-1180 against the global benthic $\delta^{18}O$ stack LR04 (Lisiecki and Raymo, 2005). The final age model was built using the software Bacon 2.3 (Blaauw and Christen, 2011). We revised the original age model to improve the chronology of Marine Isotope Stages (MIS) 9a and 8 (Fig. S1-3). Two original tie-points dragging features of MIS 9a and 8 to younger ages were removed, and a new tie point was included at 1612 cm core depth (see Text 1, Fig. S1-3, and Table S1 in *Supporting Information*). Additionally, we recalibrated the radiocarbon ages against the Marine20 calibration curve (Heaton et al., 2020). The final age model was built in Bacon 2.3 using the same setup as the original one. A comparison between the original and revised age models can be found in the Supporting Information, Fig. S2-3.

3.3. Mg/Ca analyses in foraminifera shells

We reconstructed the WTSA SST variability using the Mg/Ca composition measured in shells of planktonic foraminifera *Globigerinoides ruber* (white). Because of its ecological preferences, *G. ruber* (white) has been largely used in SST reconstructions of the western tropical Atlantic (e.g., Nascimento et al., 2022; Santos et al., 2022; Schmidt et al., 2006, 2004; Venancio et al., 2020; Weldeab et al., 2006). Several studies support that *G. ruber* (white) is a mixed-layer dwelling foraminifera with a preference for warm waters (Kucera, 2007; Lessa et al., 2020; Rebotim et al., 2017; Schmuker and Schiebel, 2002) (See Text 2 in the *Supporting Information* for details). Sediment traps moored in the WTSA show no seasonal variation in *G. ruber* (white) flux to the seafloor (Jonkers and Kučera, 2015; Žarić et al., 2005). A global planktonic foraminifera model corroborates these empirical results, suggesting that in the tropics, *G. ruber* (white) records the annual average SST (Fraile et al., 2009). Assuming that changes in environmental conditions determining calcification depth and seasonal preferences of *G. ruber* (white) have been invariant over the studied period, our Mg/Ca-based SST reconstructions are expected to record the annual average SST of the WTSA.

G. ruber (white) sampling resolution varied between 2 and 4 cm throughout the core. Twenty shells of *G. ruber* (white, 250-300 μm) were handpicked per sample. Our samples comprised *G. ruber* (white) *senso strictu* and *senso lato* morphotypes. Foraminiferal counting in 35 samples covering the first 30 kyr of GL-1180 indicates the prevalence of *G. ruber* (white) *senso strictu* (85 ± 5%, unpublished). Assuming that this prevalence dominates downcore, we rule out any substantial temperature bias related to differences in the mean calcification depths of these two morphotypes (e.g., Kearns et al., 2023; Steinke et al., 2005) (see Text 2 in the *Supporting Information* for details). The Mg/Ca analysis in the shells of *G. ruber* (white) followed the same cleaning protocol described in Nascimento et al. (2022) and Santos et al. (2022), which was based on Barker et al. (2003). Each sample was cleaned with water, methanol, hot hydrogen peroxide solution, and weak acid. No reductive step was applied. After dissolution in diluted HNO_3, measurements were performed using an inductively coupled plasma optical emission spectrometer (ICP-OES) (Agilent Technologies, 700 Series) with an autosampler (ASX-520 Cetac) at the MARUM-Center for Marine Environmental Sciences, University of Bremen. Fe, Mn, and Al were measured to monitor contamination by Mg-Fe oxide coatings and clay minerals. The calibration series consisted of one blank and five multi-element standards containing between 20 and 80 parts per million (ppm) of Ca prepared from a mixed standard purchased from SCP Science, France. An external standard also from SCP science, as well as commercial standards ECRM 752-1 (Bureau of Analysed Standards, Great Britain) and Reinstoff Nr. 3 (Bundesanstalt für Materialforschung und –Prüfung, Germany) were used to verify the accuracy of the measurements and to allow inter-laboratory comparison.

The average Mg/Ca of the external standard, which has a theoretical Mg/Ca value of 2.96 mmol/mol, was 2.97 ($\sigma \pm 0.01$) mmol/mol ($n = 127$) during our measurements. The average Mg/Ca of ECRM 752-1 was 3.88 ($\sigma \pm 0.02$) mmol/mol ($n=8$). The certified value is 3.9 mmol/mol, but some Mg contained in silicates is not released with our preparation method (Greaves et al., 2005). The average Mg/Ca of Reinstoff Nr. 3, which has a certified value of 0.800, was 0.811 ($\sigma \pm 0.004$) ($n=8$). The average Al/Ca, Mn/Ca, and Fe/Ca ratios in our samples were 0.05, 0.06, and 0.37 mmol mol^{-1}, respectively. The low correlation between Mg/Ca and Al/Ca ($r^2 = 0.07$), Mn/Ca ($r^2 = 0.11$), and Fe/Ca ($r^2 = 0.01$) (Fig. S4-6) suggests that our measurements are not affected by clay minerals or Mg-Fe oxides coatings (see Text 3 in *Supporting Information* for details). Samples with an Al/Ca ratio higher than 0.3 mmol mol^{-1} or having Mg/Ca values outside 4σ of the mean were discarded (5 samples in total). As sediment core GL-1180 was retrieved from a depth ca. 3000 m above the current lysocline depth in the Brazilian margin (Dittert and Henrich, 2000), and glacial-interglacial oscillations of the lysocline depth show a range of ca. 1000 m (Curry and Lohmann, 1986), we assume no substantial effect of calcite dissolution on foraminiferal Mg/Ca ratios in this core. In order to compare our results to records where samples were prepared using reductive cleaning, we primarily discuss SST variability rather than compare absolute values.

The Mg/Ca ratio of *G. ruber* (white) shows a temperature sensitivity of ca. 6% ± 0.8 per °C, a salinity sensitivity of 3.3 ± 2.2 % per PSU, and a pH sensitivity of -8.3% ± 7.7 per 0.1 pH unit (Gray et al., 2018). Although glacial-interglacial changes in the open ocean salinity may represent only a minor effect on reconstructed SST, the bias associated with pH variations can be substantial, with a combined effect on Mg/Ca-based SST reconstructions of ca. 1.5 °C (Gray and Evans, 2019). Accordingly, SST was calculated using the species-specific Mg/Ca-temperature equation of Gray and Evans (2019) for *G. ruber* (white). This equation corrects the effect of salinity and pH of seawater on the Mg/Ca values of foraminifera shells. To account for the salinity effect, the method considers the modern salinity of the study region plus the average ocean surface salinity anomaly between the Last Glacial Maximum and modern. The salinity anomaly is scaled to sea level changes using the sea level stack from Spratt and Lisiecki (2016). To account for the pH effect, we applied the atmospheric CO_2 protocol, which uses an atmospheric CO_2 concentration stack derived from ice cores (Bereiter et al., 2015) to reconstruct past changes in ocean pH. For the CO_2 protocol, we input the modern alkalinity and pCO_2 disequilibrium at the study region. The input parameters were 36.3 for salinity (Zweng et al., 2019), 2380 µmol kg^{-1} for alkalinity (Lee et al., 2006), and 25 µatm for pCO_2 disequilibrium (Takahashi et al., 2009). The mean 1σ uncertainty for all SST estimates derived from the Mg/Ca-SST calibration was 0.8 °C.

Using the Mg/Ca-based SST record to remove the effect of temperature on the $\delta^{18}O$ of *G. ruber* (white) from GL-1180 (Nascimento et al., 2021), we were able to calculate the $\delta^{18}O$ of seawater, which, corrected by changes in the continental ice volume ($\delta^{18}O_{SW-IVF}$), is a proxy for sea surface salinity changes (see Text 4 in the *Supporting Information* for details).

4. Results

GL-1180 Mg/Ca records of *G. ruber* (white) for the last deglaciation and Marine Isotope Stage (MIS) 5e have been previously published by Santos et al. (2022) and Nascimento et al. (2022), respectively (Fig. 2b). Here we present the complete 300 kyr-long Mg/Ca and reconstructed SST records from sediment core GL-1180 (Fig. 2b, c). These records encompass the last three glacial-interglacial cycles, from MIS 9 to MIS 1, with an unprecedented mean resolution for the study region of approximately 0.6 kyr among adjacent samples (Fig. 2b, c). Mg/Ca values vary between 3.79 and 5.52 mmol mol^{-1}, with an average of 4.46 mmol mol^{-1} (Fig. 2b). This resulted in SST ranging between 23.8 and 29.3 °C, with an average of 26.4 °C (Fig. 2c). The average SST value of the three uppermost top core samples from GL-1180 (26.7 ± 0.0 °C) (Santos et al., 2022) is in excellent agreement with the pre-industrial annual average SST (26.9 °C) for this site (Rayner et al., 2003), indicating that our SST reconstruction is faithfully representing the modern environmental conditions of the study region.

The SST record shows a clear glacial-interglacial pattern (Fig. 2a, c). The transition from glacial MIS6 to interglacial MIS5e, i.e., glacial Termination II, shows the largest SST variation (ca. 3.5 °C), followed by Terminations III and I, with SST increases of ca. 3 °C and ca. 2 °C, respectively. A remarkable feature of our SST record is the occurrence of four long-term warm events during the last three recorded glacial intervals, hereafter called glacial warm events (GWE) (Fig. 2c). In general, these GWE show average SST values similar to the current interglacial period and were superimposed by short-term millennial-scale SST variability (Fig. 2c). These glacial warm events are observed during MIS 3/2 (GWE1), MIS 5/4 (GWE2), MIS 6 (GWE3), and MIS 8 (GWE4). These GWE occurred between ca. 280-260 (GWE4), 160-143 (GWE3), 75-60 (GWE2), and 40-24 (GWE1) ka. They are marked by temperatures substantially higher than the subsequent glacial maxima conditions (Fig. 2c). In turn, these warm events shortened the duration of glacial maxima conditions in the WTSA.

After the warm period characteristic of MIS 9a (between ca. 290 and 280 ka), the WTSA stays warm until ca. 260 ka, indicating the occurrence of the GWE4. The SST descends towards glacial conditions only at ca. 256 ka, interrupted by a millennial-scale warm peak centered at 255 ka. The average SST during the GWE4 was 26.4 ± 0.6 °C. The GWE3, within the MIS 6, is marked by a steady SST increase, superimposed by high-frequency millennial-scale variability, beginning from ca. 180 ka. The SST rises sharply at ca. 160 ka until peak temperatures of ca. 29.5

°C at 145 ka, after which SST decreases around 3°C back to cold glacial maximum conditions at ca. 143 ka. Considering the interval between 160-143 ka, the average SST during the GWE3 was 26.6 ± 0.6 °C. The GWE2, between ca. 75 and 60 ka, begins at the end of MIS 5 and lasts throughout MIS 4. The average SST during this period was 26.8 ± 0.7 °C, which is similar to core top values (26.7 ± 0.0 °C) and ca. 1.5°C higher relative to subsequent cold conditions between 60 and 40 ka, when the average temperature value was 25.3 ± 0.5 °C. The GWE1 was recorded during MIS 3/2, with the warming of the WTSA starting at 40 ka. Between 40 and 30 ka, GWE1 is marked by a high-frequency variability with notable millennial-scale SST peak at 35 ka and a sharp drop at 30 ka. The SST decreases back to cold conditions only at ca. 24 ka, i.e., within the Last Glacial Maximum. The average SST during the GWE1 was 26.5 ± 0.5 °C, approximately 1 °C higher relative to the subsequent Last Glacial Maximum conditions in the region of GL-1180.

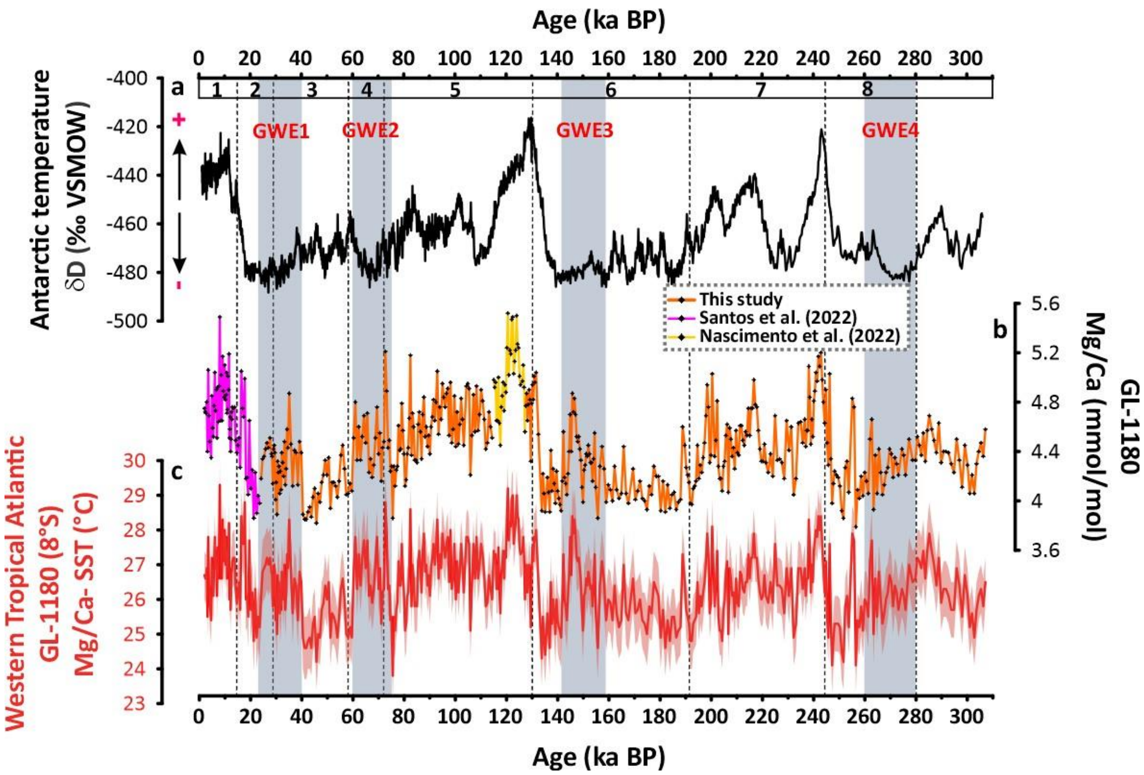

Figure 2: Mg/Ca ratio and Mg/Ca-based sea surface temperature (SST) record of sediment core GL-1180 (western tropical South Atlantic) plotted against Antarctic stable hydrogen isotopes (δD) record as a proxy for Antarctic air temperature. a) δD from European Project for Ice Coring in Antarctica (EPICA) Dome C (Jouzel et al., 2007) on the Antarctic ice core chronology (AICC2012) (Bazin et al., 2013; Veres et al., 2013). b) Mg/Ca ratio of *Globigerinoides ruber* (white). Orange, magenta, and yellow curves depict the dataset published in this study, Santos

et al. (2022), and Nascimento et al. (2022), respectively. c) *G. ruber* (white) Mg/Ca-based SST record from sediment core GL-1180 (this study). SST was estimated using the species-specific Mg/Ca-temperature equation for *G. ruber* (white) from Gray and Evans (2019). The curve envelope shows the variable 1σ uncertainty (Gray and Evans, 2019). Vertical gray bars highlight the four glacial warm events (GWE) 1 to 4. Vertical dotted lines separate Marine Isotope Stages indicated by numbers along the top x-axis.

5. Discussion

5.1. Mg/Ca-based SST records from tropical latitudes

The GL-1180 Mg/Ca-based SST reconstruction shares much of its glacial-interglacial variability with Mg/Ca-based SST reconstructions from the western tropical North Atlantic ODP Site 999A (Figs. 1a, 3a,b) (Schmidt et al., 2006) and the eastern tropical Atlantic cores GeoB1105-4 and GeoB1112-4 (Figs. 1a, 3d,e) (Nürnberg et al., 2000). On the other hand, the SST variability of core GL-1180 is remarkably distinct from Mg/Ca-based SST reconstruction derived from sediment core M125-55-7 (20°S) (Figs. 1a, 3b, c), also from the WTSA (Hou et al., 2020). The SST record from M125-55-7 was the first published 300 kyr-long Mg/Ca-based SST record from the WTSA and is the nearest record to GL-1180 with a comparable stratigraphic extent. However, the SST record from M125-55-7 does not present an obvious glacial-interglacial oscillation as observed in GL-1180 (Fig. 3b, c). Regional oceanographic features may be responsible for the difference between the SST records from these cores. Sediment core M125-55-7 was retrieved within the local Vitória Upwelling system (Aguiar et al., 2014; Schmid et al., 1995). This small upwelling system probably intensifies during interglacial summer months (Lessa et al., 2019, 2017). This intensification would decrease the interglacial annual average SST in the region of M125-55-7 by pumping up cold subsurface water to the mixed layer, dampening the glacial-interglacial SST contrast. Such dampening could have been further amplified if there was a summer bias in the flux of *G. ruber* (white) in the recovery region of sediment core M125-55-7, as implied by a sediment trap dataset (Venancio et al., 2017, 2016).

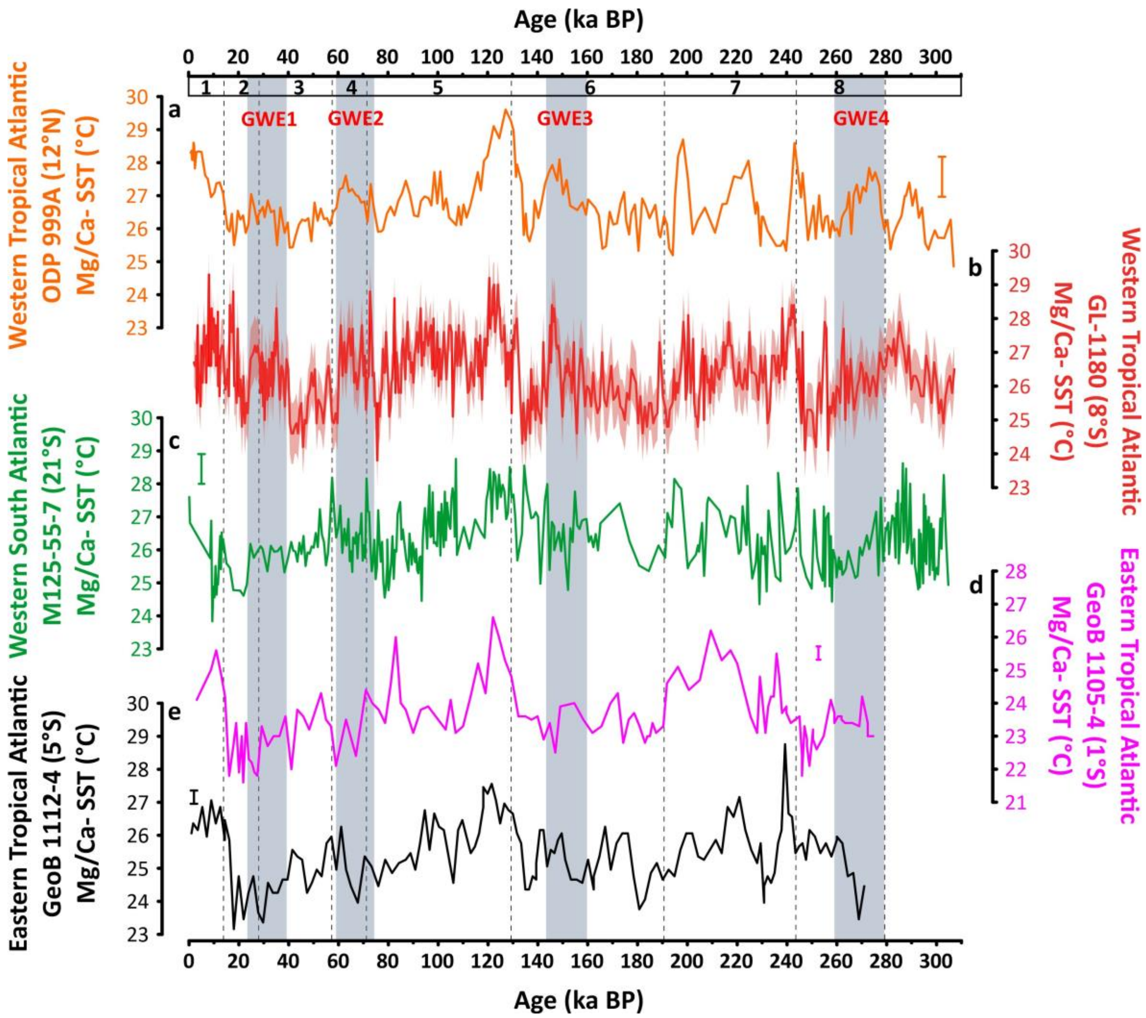

Figure 3: Mg/Ca-based sea surface temperature (SST) records from the tropical Atlantic (see Figure 1 for site locations). a) *G. ruber* (white) Mg/Ca-based SST record from Site ODP 999A from the western tropical North Atlantic (Schmidt et al., 2006). b) *Globigerinoides ruber* (white) Mg/Ca-based SST record from sediment core GL-1180 (this study). SST for core GL-1180 was estimated using the species-specific Mg/Ca-temperature equation for *G. ruber* (white) from Gray and Evans (2019). The envelope of the curve shows the variable 1σ uncertainty. c) *G. ruber* (white) Mg/Ca-based SST record from sediment core M125-55-7 from the western tropical South Atlantic (Hou et al., 2020). d and e) *Trilobatus sacculifer* Mg/Ca-based SST record from sediment cores GeoB1105-4 and GeoB1112-4 from the eastern tropical Atlantic (Nürnberg et al., 2000). The SST values and uncertainties, as well as the chronology of records, follow the original studies. Vertical gray bars indicate glacial warm events (GWE) 1 to 4. Vertical dotted lines separate the Marine Isotope Stages indicated by the numbers in the top x-axis.

A remarkable feature of our Mg/Ca-based SST reconstruction is the unusual long-term GWE. These warm events are long-term periods of high SST values relative to the subsequent glacial maxima. They occur during full glacial conditions indicated by the surface temperature record of Antarctica (Fig. 2), which closely mirrors the global temperature variability during glacial cycles (Brook and Buizert, 2018). The magnitude and duration of these GWE seem to be unique features of the western tropical Atlantic. In the eastern equatorial Atlantic, warm events were observed during the last two glacial periods (Fig. 3c, d) (Nürnberg et al., 2000), but with lower magnitude and not synchronous with the warm events found in the WTSA. SST variability in the eastern equatorial Atlantic is thought to be strongly influenced by precessional changes in the strength of the equatorial upwelling (McIntyre et al., 1989). In contrast, GWE similar to those observed in our record were found in the SST reconstruction from ODP Site 999A (western tropical North Atlantic; Schmidt et al., 2006), suggesting that these records may have been modulated by the same forcing(s) (Fig. 3a, b). While the SST record from Site 999A is thought to be biased toward boreal summer insolation (Schmidt et al., 2006), no evidence of such seasonal bias is present in Mg/Ca-based SST record from core GL-1180 (e.g., Nascimento et al., 2022). Assuming our SST reconstruction represents annual averages, climatic forcings other than precessional-driven seasonal insolation must have caused the GWE in the western tropical Atlantic.

5.2. Glacial-interglacial greenhouse gases variability and western tropical South Atlantic SST

Based on the climate sensitivity of the tropical Pacific, previous studies have shown that the long-term glacial-interglacial SST variability in the tropics is strongly controlled by atmospheric GHG concentration (Lea, 2004; Dyez and Ravelo, 2013; Tachikawa et al., 2014). In light of these studies, we estimated the climate sensitivity of the WTSA over the last 300 kyr (Fig. 4b). The radiative forcing from GHG relative to pre-industrial conditions (ΔRF_{GHG}), derived from atmospheric CO_2 and CH_4 concentrations (Loulergue et al., 2008; Lüthi et al., 2008), was calculated at 2 kyr resolution using the equation from Ramaswamy et al. (2001). When plotted together, our SST reconstruction shares an outstanding similar glacial-interglacial variability with the ΔRF_{GHG} (Fig. 4b). However, remarkable deviations between these two records occur during the GWE1-4. Figure 4 shows that GWE occur even when the ΔRF_{GHG} was steadily low (e.g., GWE3) or decreasing (e.g., GWE1-2). Another notable decoupling between our SST record and ΔRF_{GHG} occurred during MIS 1, the so-called Holocene temperature conundrum (Liu et al., 2014), which is out of the scope of this study.

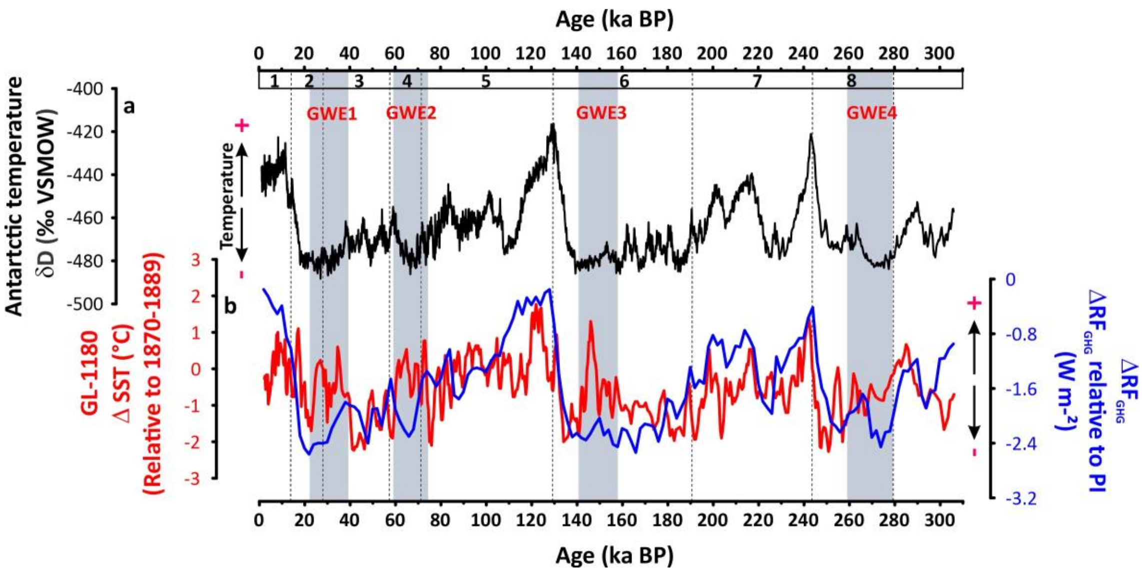

Figure 4: Sea surface temperature (SST) from sediment core GL-1180 plotted alongside radiative forcing from greenhouse gases (ΔRF_{GHG}) and Antarctic stable hydrogen isotopes (δD) record as a proxy for surface air temperature. a) Stable hydrogen isotopes (δD) from European Project for Ice Coring in Antarctica (EPICA) Dome C (Jouzel et al., 2007) plotted on the Antarctic ice core chronology (AICC2012) (Bazin et al., 2013; Veres et al., 2013) as a reference for glacial-interglacial temperature variations. b) Three-points running average of *Globigerinoides ruber* (white) Mg/Ca-based SST from sediment core GL-1180 relative to climatological pre-industrial SST value taken near site GL-1180 (Rayner et al., 2003) (red line); ΔRF_{GHG} calculated from CO_2 (Lüthi et al. 2008) and CH_4 (Loulergue et al., 2008) (blue line) in the Antarctic ice core chronology (AICC2012) (Bazin et al., 2013; Veres et al., 2013). The ΔRF_{GHG} is computed at two kyr-resolution using the standard radiative forcing relationships (Ramaswamy et al. 2001) relative to pre-industrial (PI) levels of 280 ppm and 700 ppb for CO_2 and CH_4, respectively. Vertical gray bars highlight the glacial warm events (GWE) 1 to 4. Vertical dotted lines separate the Marine Isotope Stages indicated by the numbers in the top x-axis.

The slope between ΔRF_{GHG} and SST from GL-1180 yields a climate sensitivity of the WTSA SST of 0.56 (±0.1) °C (W m^{-2})$^{-1}$, with r = 0.4 ($p < 0.05$) (Fig. 5). This value is approximately half the climate sensitivity of ca. 1 °C observed in the tropical Pacific (e.g., Lea, 2004; Dyez and Ravelo, 2013; Tachikawa et al., 2014), but it agrees with an area-weighted climate sensitivity ca. 0.4 °C (W m^{-2})$^{-1}$ estimated for the latitudinal band between 0° and 10° south (Rohling et al., 2012). The lower climate sensitivity of the WTSA relative to the tropical Pacific can be partially explained by the GWE. The increased spread of SST values caused by the GWE reduces the linear regression slope, hence the WTSA climate sensitivity. No correlation between SST and ΔRF_{GHG} is observed during glacial periods (Fig. 5). On the other hand, when considering only the interglacial periods, including glacial terminations, the WTSA climate sensitivity rises to 0.72 (±0.2) °C (W m^{-2})$^{-1}$ (r = 0.4) ($p < 0.05$) (Fig. 5). The enhanced climate sensitivity of our study region during periods of elevated GHG concentration agrees with recent results from the tropical Pacific Ocean, suggesting a nonlinear sensitivity of SST to GHG (Lo et al., 2017).

Given a climate sensitivity of 0.72 °C (W m^{-2}), an average RF_{GHG} rise of ~2.5 W m^{-2} during glacial terminations corresponds to an SST increase of ~2 °C in the WTSA. This value accounts for over half of the SST increase during terminations II and III and the total increase during the last glacial termination (Santos et al., 2022). Therefore, considering the glacial-interglacial covariation between our SST and ΔRF_{GHG} and the climate sensitivity of the WTSA, we suggest that the glacial-interglacial variability of atmospheric CO_2 associated with full changes in the Earth's climate largely explains the glacial-interglacial pattern of the WTSA SST. This corroborates the previous notion that the long-term SST in the tropics is mainly controlled by GHG orbital-scale variability. However, the presence of GWE suggests that additional forcing(s) are driving the WTSA SST.

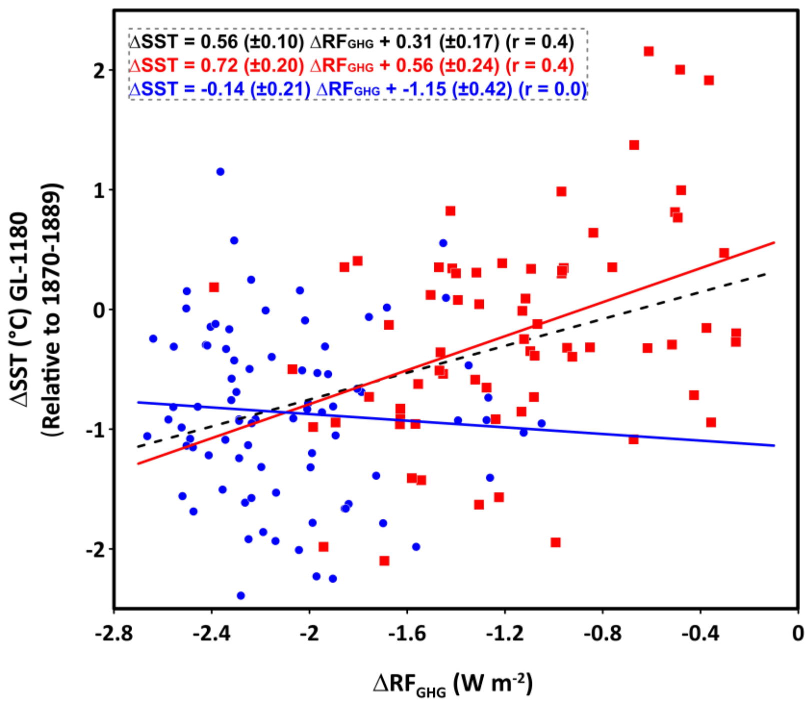

Figure 5: Linear regressions between sea surface temperature anomaly (ΔSST) relative to pre-industrial (1870-1889) value and radiative forcing from greenhouse gases (ΔRF_{GHG}). We used the climatological pre-industrial SST of 26.9°C near site GL-1180 (Rayner et al., 2003). The radiative forcing is computed from standard radiative forcing relationships (Ramaswamy et al., 2001) relative to preindustrial levels of CO_2 (280 ppm) and CH_4 (700 ppb). CO_2 (Lüthi et al., 2007) and CH_4 (Loulergue et al., 2008) records are in the Antarctic ice core chronology (AICC2012) (Bazin et al., 2013; Veres et al., 2013). SST and greenhouse gases were interpolated at two kyr resolution. Red squares depict interglacial periods and glacial-interglacial transition. Blue circles depict glacial periods. Linear regressions: (i) between the full 300 kyr-long SST and GHG records (black dotted line); (ii) including only interglacials and glacial-interglacial transitions (red squares; red line); (iii) including only glacials (blue circles; blue line).

5.3. Insolation forcing on western tropical South Atlantic SST

Obliquity is the only orbital forcing that substantially affects the annual mean insolation at a given latitude (Berger et al., 2010; Loutre et al., 2004). The annual mean insolation is in anti-phase with obliquity within the latitudinal band between ca. 43° N-S, i.e., the mean insolation is high [low] during periods of low [high] obliquity (Loutre et al., 2004). The annual mean insolation has low amplitude (e.g., ca. 3 W m^2 around the latitude of GL-1180); however, because the upper ocean integrates direct insolation forcing over several years, the annual insolation may produce significant changes in the SST (Cortijo et al., 1999). For example, the annual mean insolation has been previously evoked to explain mid-to-low latitudes orbital-scale SST variations (Cortijo et al., 1999; Pahnke and Sachs, 2006; Santos et al., 2017). Indeed, the long-term GWE are aligned to periods of high annual mean insolation (low obliquity) (Fig. 6a, d). This synchronicity could point to annual mean insolation as the main driver of these events in the WTSA. The annual insolation has been thought to have caused the early warming of the Brazil Current (BC) preceding the last two glacial terminations, as observed in a SST reconstruction from sediment core GL-1090 in the western South Atlantic (Figs. 1a, 6e) (Santos et al., 2017). In turn, the early warming of the BC during MIS 6 and 3 agrees, within chronological uncertainty, with the beginning of the GWE3 and 1 in GL-1180 (Fig. 6d, e), respectively, suggesting that a similar mechanism controlled these records.

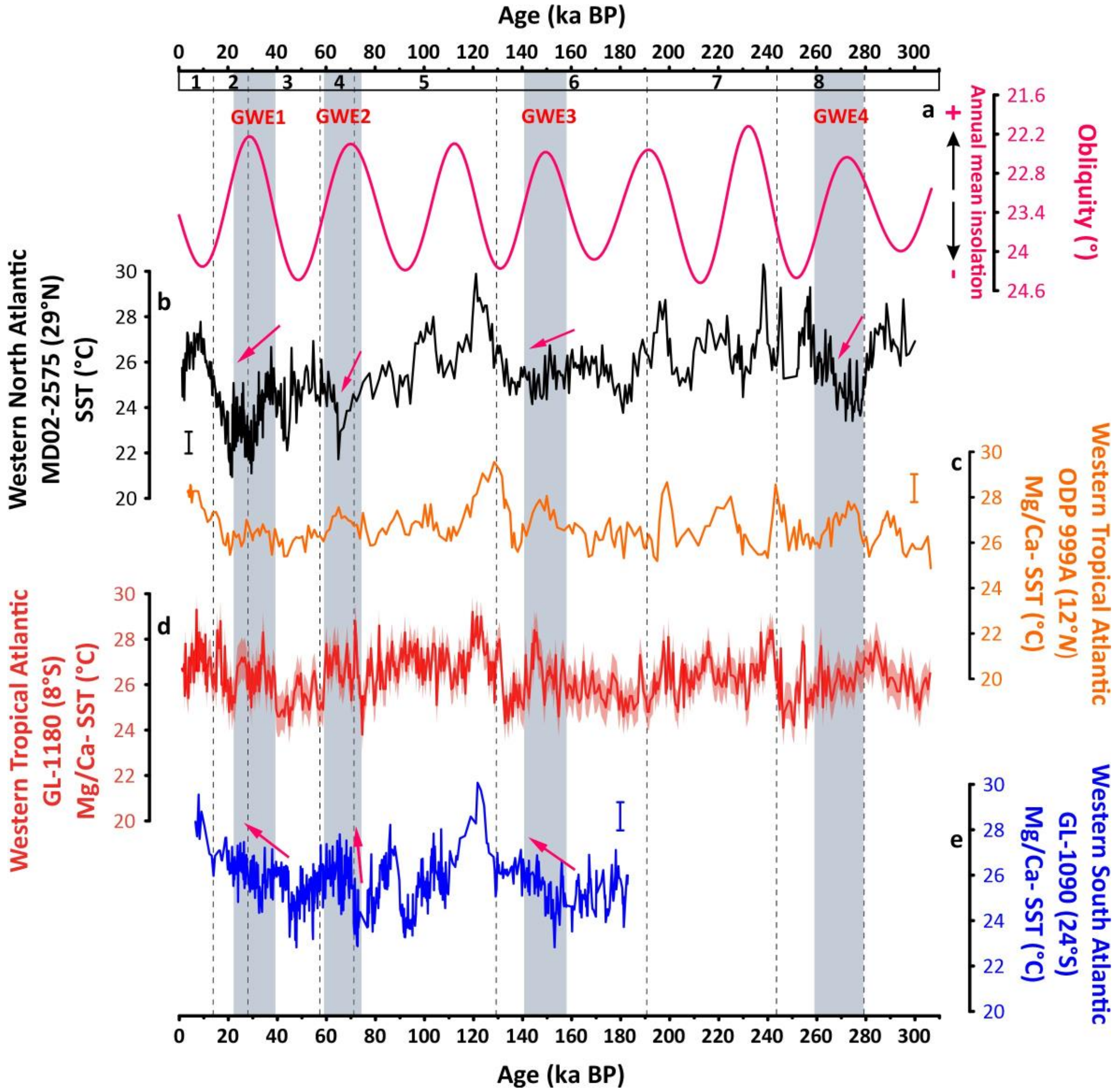

Figure 6: Western tropical Atlantic sea surface temperature (SST) records plotted alongside western subtropical records. a) Obliquity as an indicator of the annual mean insolation variability between ca. 43° N-S (Berger and Loutre, 1991). Low [high] obliquity indicates high [low] annual mean insolation. b) *Globigerinoides ruber* (white) Mg/Ca-based SST record from sediment core MD02-2575 from the western subtropical North Atlantic (Gulf of Mexico) (Ziegler et al., 2008). c) *G. ruber* (white) Mg/Ca-based SST record from Site ODP 999A from the western tropical North Atlantic (Schmidt et al., 2006). d) *G. ruber* (white) Mg/Ca-based SST record from sediment core GL-1180 (red line) (this study). SST for core GL-1180 was estimated using the species-specific Mg/Ca-temperature equation for *G. ruber* (white) from Gray and Evans (2019). The envelope of the curve shows the variable 1σ uncertainty. e) *G. ruber* (white) Mg/Ca-based SST record from sediment core GL-1090 from the western subtropical South Atlantic (Santos et al., 2017). The SST values, uncertainties, and chronology of the records follow the original studies. Vertical gray bars are aligned with the glacial warm events (GWE) 1 to 4. Vertical dotted lines separate the

Marine Isotope Stages indicated by the numbers in the top x-axis. The pink arrows illustrate the trend of the subtropical SST records during the GWE.

If the annual mean insolation was the leading cause of the GWE, these events should simultaneously occur in the latitude band between ~43° N-S. However, the GWE seem to be restricted to the western tropical (South) Atlantic margin, namely ODP Site 999A (Schmidt et al., 2006), GL-1180 (this study), and GL-1090 (Santos et al., 2017) (Fig. 6c-e). Interestingly, there is no evidence of propagation of these glacial warmings along the western Atlantic north of ODP 999A, as implied by the high-resolution Mg/Ca-based SST record from sediment core MD02-2575 at 29°N in the Gulf of Mexico (Figs. 1a, 6b) (Ziegler et al., 2008). In fact, the SST from MD02-2575 decreases during the GWE despite the high annual mean insolation, as indicated by low obliquity values (Fig 6a, b). Nürnberg et al. (2008) note that the SST records from MD02-2575 and ODP Site 999A deviate during glacial conditions (Fig 6b, c). The same observation seems true when comparing the SST records from MD02-2575 and GL-1180 (Fig 6b, d). Therefore, whatever the main forcing responsible for the GWE, it seems to prevent the northward spread of the warming beyond ODP Site 999A, which would not be expected with annual mean insolation as the dominant driver. Numerical simulations reinforce the controversial role of annual mean insolation on tropical SST, indicating no substantial response to this forcing in the tropical Pacific (Tachikawa et al., 2014; Timmermann et al., 2007). Therefore, although it would be tempting to say that the annual mean insolation is the main driver of the GWE in the SST record from GL-1180, the available evidence suggests the opposite. Still, given the correspondence between the GWE and high values of annual mean insolation, we speculate that it may have amplified the warming.

5.4. Long-term AMOC variability and the western tropical South Atlantic SST

Based on the benthic $\delta^{13}C$ gradient ($\Delta\delta^{13}C$) between records from the Atlantic and the Pacific oceans, Lisiecki et al. (2008) inferred long-term changes in the NADW formation rate over the last 425 kyr. The authors suggest that the minima in $\Delta\delta^{13}C$ primarily reflect a reduction in the mixing ratio between NADW and Southern Ocean Water at the mid-depth of the Atlantic due to weaker and/or shallower AMOC. Recent studies have shown that $\delta^{13}C$ is an excellent proxy for water mass mixing, and although it is not the best indicator of AMOC advection rate, it is also sensitive to the strength of the deep overturning (Muglia and Schmittner, 2021; Pöppelmeier et al., 2023). In fact, despite some disagreements relative to the different resolution of records and the sensitivity of proxies, $\Delta\delta^{13}C$ shares much of its long-term variability with $^{231}Pa/^{230}Th$ records, a proxy for deep AMOC strength (Fig. S7). Therefore, we use $\Delta\delta^{13}C$ as an indicator for changes in AMOC strength. A similar approach had been previously applied by Mix and Fairbanks (1985) and Raymo et al. (1990).

As implied in the bipolar seesaw mechanism, a decline in AMOC strength reduces the northward cross-equatorial heat transport and increases low latitude SST (e.g., Mix et al., 1986; Crowley, 1992; Rühlemann et al., 1999; Stocker and Johnsen, 2003). Figure 7a shows our SST record plotted against $\Delta\delta^{13}C$. Despite the distinct temporal resolution between both records, there is a generally good correspondence between high SST and low $\Delta\delta^{13}C$ throughout most of the last 300 kyr. This agreement points to a long-term bipolar seesaw mechanism, in which periods of weakened North Atlantic deep convection, as indicated by low $\Delta\delta^{13}C$, imply a reduction in the cross-equatorial heat transport toward the North Atlantic, hence warming the upper WTSA. Indeed, Lisiecki et al. (2008) suggested the operation of such a mechanism by showing that the SST record from ODP Site 999A, in the western tropical North Atlantic, is in anti-phase with $\Delta\delta^{13}C$ and mid-latitude North Atlantic SST record from DSDP Site 607 (Ruddiman et al., 1989; Ruddiman and McIntyre, 1981). However, this conclusion is undermined by a possible bias in the SST record from Site 999A toward boreal summer (Schmidt et al., 2006; Lisiecki et al., 2008).

Given that the SST record of GL-1180 represents the annual mean, we further investigate the hypothesis of an orbital-scale bipolar seesaw driving GWE in the WTSA by calculating the SST gradient (ΔSST) between the GL-1180 and MD02-2575 (Ziegler et al., 2008). The Mg/Ca-based SST record from MD02-2575 is also related to the annual mean temperature (Nürnberg et al., 2008). This core was retrieved from the Gulf of Mexico at 29 °N (Fig. 1), directly under the influence of Loop Current (LC), a major component of the upper limb of the AMOC in the North Atlantic (Johns et al., 2002) (Fig. 1). During glacial periods, ΔSST between GL-1180 and MD02-2575 exhibits high values concurrent with weakened North Atlantic deep convection (i.e., low $\Delta\delta^{13}C$) during the four GWE (Fig. 7 b). High ΔSST values during GWE agrees with the deviations between the SST records from MD02-2575 and ODP 999A observed during glacial periods (Nürnberg et al., 2008). Therefore, the ΔSST record further corroborates the idea that these warm events were caused mainly by orbital-scale reduction of the cross-equatorial heat transport by the AMOC, resulting in a thermal bipolar seesaw between the western tropical (South) Atlantic and mid-latitudes of the North Atlantic. The reduction in the northward cross-equatorial transport is further reinforced by the build-up of salinity in the WTSA during the GWE 1 to 3, as indicated by the $\delta^{18}O_{SW-IVF}$ (Fig. 7d), which was calculated by correcting $\delta^{18}O$ of *G. ruber* from GL-1180 (Nascimento et al., 2021) by the effect of SST and continental ice volume changes (see Text 4 in *Supporting information* for details). The orbital-scale SST variability from MD02-2575 is thought to be mostly driven by glacial-interglacial changes in ice volume and the dynamics of the ITCZ (Ziegler et al., 2008). Here, we suggest that orbital-scale SST variability in the Gulf of Mexico is also affected by a long-term bipolar seesaw operating in the Atlantic. Periods of strong AMOC are associated with a strong LC and enhanced advection of warm Caribbean waters northward into the Gulf of Mexico. The opposite must occur during periods of weak AMOC.

Along with the annual mean insolation, Santos et al. (2017) propose a long-term bipolar seesaw as an additional mechanism to explain the warming of the BC preceding the last two glacial terminations indicated by the SST record from GL-1090 (Fig. 6e). Santos et al. (2017) suggested that a long-term thermal bipolar seesaw would not require an abrupt decline or shutdown of the AMOC as during millennial North Atlantic cold events. Instead, they suggest that a progressive long-term change in the AMOC strength would reorganize meridional heat distribution across the Atlantic Ocean. Observational data show that subtle decadal to centennial timescale variability of the North Atlantic deep convection reverberates on the western tropical Atlantic SST (Vellinga and Wu, 2004; Yang, 1999; Zhang et al., 2011). Based on the evidence presented here, we propose that the long-term bipolar seesaw was the main mechanism driving the early warming of the BC preceding the last two glacial terminations. Ultimately, we suggest that, even subtly, the long-term bipolar seesaw caused by orbital-scale variability of the AMOC has interhemispheric thermal reverberations broadly recorded in the western tropical (South) Atlantic margin.

The variability of the North Atlantic deep convection, as indicated by $\Delta\delta^{13}C$, also seems consistent with some SST features of GL-1180 during interglacial periods. For example, during the MIS5e, the WTSA cooling parallels to increasing $\Delta\delta^{13}C$, but almost 10 kyr before the RF_{GHG} started to decline from its interglacial plateau (~280 ppm) (Fig. 4b). This early cooling of the WTSA may have been caused by enhanced NADW production towards the end of the Last Interglacial period (Fig. 7a) (Crowley, 1992). Although ΔSST points to a strong AMOC since the beginning of MIS 5e (Fig. 7b), evidence from the deep NE Atlantic supports a later resumption of the deep overturning in the Nordic Seas and overflow of NADW into the Atlantic basin during the Last Interglacial (Deaney et al., 2017; Hodell et al., 2009).

The millennial-scale bipolar seesaw mechanism is associated with an anti-phase temperature evolution between Greenland and Antarctica, as indicated by ice core records (Blunier et al., 2001; Buizert et al., 2015; Members, 2006). In contrast, no antiphase temperature oscillations between Greenland and Antarctica are observed during the last two GWE in the western tropical Atlantic. Glacial boundary conditions are marked by the equatorward displacement of the Subtropical Front as the meridional temperature gradient between low and high latitudes steepens (e.g., Bard and Rickaby, 2009; Toggweiler et al., 2006). Accordingly, we assume that a substantial oscillation in the meridional heat transport by the AMOC would be required to relocate the fronts and warm polar regions. This seems to be the case for the abrupt millennial events (Pedro et al., 2018; Pinho et al., 2021). However, it is likely that a subtle and progressive long-term weakening of the North Atlantic deep convection, as proposed here, could not cause such meridional readjustment in the fronts position associated with the glacial conditions. Besides, cold glacial NADW was continuously formed in high latitudes of the North Atlantic, and the eventual upwelling of this water mass in the Southern Ocean favored maintaining cold conditions around Antarctica (Adkins, 2013). Additionally, the GWE were counterbalanced by a reduced RF_{GHG} due to low atmospheric CO_2 concentration (Ahn and Brook, 2008) that, together with the albedo feedback related to sea ice and continental ice sheets, may have allowed the prevalence of cold conditions towards high latitudes.

Evidence suggests that the Southern Hemisphere descends into full glacial conditions during the MIS 5/4 transition (Schaefer et al., 2015). Barker and Diz (2014) suggest synchronous interhemispheric inception into glacial conditions during this transition, resulting in a global cooling not characteristic of the bipolar seesaw. The MIS 5/4 transition was marked by a striking decrease in atmospheric CO_2 concentration (Ahn and Brook, 2008), possibly due to a shoaling of the AMOC with associated enhanced deep ocean stratification (Adkins, 2013) and higher ocean primary productivity due to the increase in dust-borne iron fertilization of the Southern Ocean (Kohfeld and Chase, 2017; Martínez-garcía et al., 2014). Despite this sharp decline in the atmospheric CO_2 concentration, MIS 4 is approximately synchronous with the GWE2 (Fig. 7a). This is consistent with previous SST reconstructions from the western tropical North Atlantic (ODP Site 999A; Schmidt et al., 2006) and western South Atlantic (Santos et al., 2017; Venancio et al., 2020). We suggest that the GWE2 in the western tropical (South) Atlantic during MIS 4 was caused by the orbital-scale bipolar seesaw, as implied by low $\Delta\delta^{13}C$ and high ΔSST (Fig. 7a, b). The slowdown of the NADW during the MIS 4 is further supported by sortable silt results (Thornalley et al., 2013). Therefore, evidence is accumulating that while most of the planet cooled during the MIS 4/5 transition, the western tropical (South) Atlantic warmed.

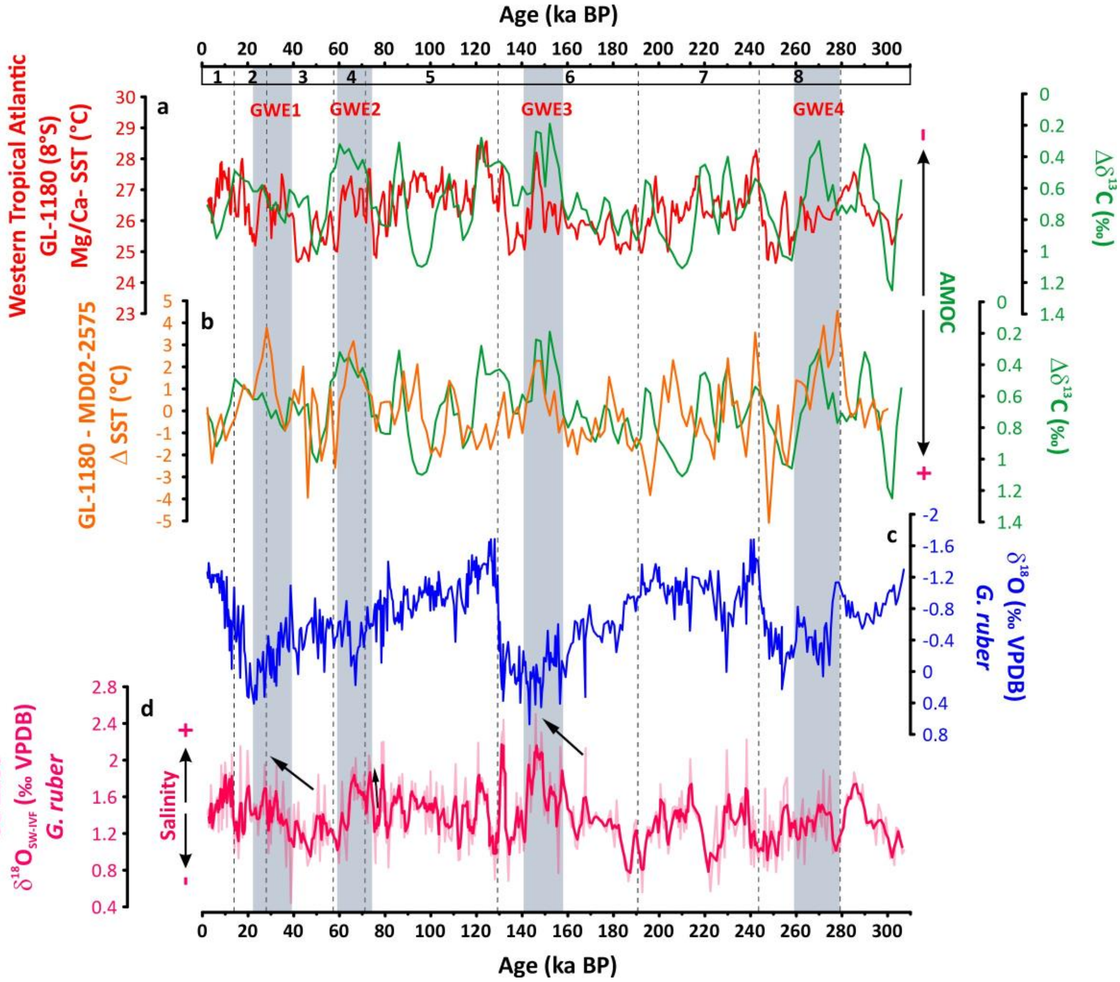

Figure 7: Evidence for an orbital-scale bipolar seesaw mechanism in the Atlantic. a) Three-points running average of *Globigerinoides ruber* (white) Mg/Ca-based SST from sediment core GL-1180 (red line) and $\delta^{13}C$ gradient ($\Delta\delta^{13}C$) between mid-depth records from the Atlantic and benthic $\delta^{13}C$ records from the Pacific Ocean (green line) (Lisiecki et al.,2008). Minima in $\Delta\delta^{13}C$ reflect a reduction in the mixing ratio of North Atlantic Deep Water at the mid-depth of the Atlantic due to weaker and/or shallower Atlantic Meridional Overturning Circulation (AMOC). b) The orange line depicts the detrended Mg/Ca-based sea surface temperature gradient (ΔSST) between sediment cores GL-1180 (this study) and MD02-2575 (Ziegler et al., 2008) plotted along with $\Delta\delta^{13}C$ (green line). For ΔSST calculation, both SST records were estimated using the species-specific Mg/Ca-temperature equation for *G. ruber* (white) from Gray and Evans (2019) and interpolated at two kyr-resolution. c) Stable oxygen isotopes ($\delta^{18}O$) of *G. ruber* (white) from GL-1180 (Nascimento et al., 2021). d) ice-volume-corrected $\delta^{18}O$ of seawater ($\delta^{18}O_{sw-ivc}$) as a proxy for relative changes in sea surface salinity (light pink line) with 3-points running average (pink). Values were reconstructed from the $\delta^{18}O$ and Mg/Ca-based temperature of *G. ruber* (white) from GL-1180 (Text 4 in *Supporting Information*). Vertical gray bars are aligned with the glacial warm events (GWE) 1 to 4. Vertical dotted lines separate the Marine Isotope Stages indicated by the numbers in the top x-axis. The black arrows illustrate the trend of the $\delta^{18}O_{sw-ivc}$ record during the GWE.

6. Conclusions

We investigated the drivers of orbital-scale variability of the western tropical South Atlantic (WTSA) sea surface temperature (SST) over the last 300 kyr. Our SST reconstruction shows a marked glacial-interglacial variability superimposed by recurrent long-term warm events within the previous three glacial periods. Our results indicate that atmospheric GHG concentration plays the leading role in modulating the glacial-interglacial WTSA SST oscillation, in agreement with previous findings from the tropical Pacific. We show that the WTSA has a sensitivity of 0.56 ± 0.1 °C (W $m^{-2})^{-1}$. This value increases if we exclude the glacial periods (0.72 ± 0.2 °C (W $m^{-2})^{-1}$), indicating that the amplitude of SST values during glacial periods reduces the slope of the linear regression and the climate sensitivity of our record.

The presented results corroborate the idea that a long-term orbital-scale bipolar seesaw operates in the Atlantic. This mechanism leads to the glacial warm events observed in the western tropical Atlantic due to a reduction in the northward heat transport by the AMOC. We hypothesize that these warm events were amplified by obliquity-driven annual mean insolation. Because of long-term bipolar seesaw mechanisms, the western tropical and South Atlantic warmed up while most of the planet cooled off during the MIS 5/4 transition. Our results imply that the western tropical Atlantic is highly susceptible to changes in the strength of the AMOC, not only on a millennial but also on an orbital-scale. The causes and further consequences of a long-term bipolar seesaw must be better explored in future studies.

7. Acknowledgments

We thank the Petrobras for providing the sediment core used in this study. This study was supported by the CAPES-ASpECTO project (grant 88887.091731/2014-01), CNPq-Aspecto (grant 429767/2018-8), CAPES-PRINT CLIMATE Project (grant 88887.310301/2018-00). I.M. Venancio acknowledges the support of FAPERJ (SEI-260003/000677/2023) (JCNE grant 200.120/2023–281226). C.M.C. acknowledges the financial support from FAPESP (grants 2018/15123-4 and 2019/24349-9), CNPq (grant 312458/2020-7), and the Alfred Wegener

Institute for Polar and Marine Research. M.C.C acknowledges the financial support from FAPESP (grants 2019/25179-0, 2022/09479-6, and 2022/06452-0). A.L.S.A. is a senior scholar CNPq (grant 302521/2017-8). We also acknowledge the partial support from the Coordenação de Aperfeiçoamento de Pessoal de Nível Superior – Brasil (CAPES) – Finance Code 001. We acknowledge the CNRS-France (Centre National de la Recherche Scientifique) support of the France-Brazil cooperation through the International Research Project SARAVA (Drivers of past changes in South Atlantic circulation and tropical South American climate).

8. Data Availability

All data presented in this manuscript are available at www.pangaea.de.

9. References

Adkins, J.F., 2013. The role of deep ocean circulation in setting glacial climates. Paleoceanography 28, 539–561. https://doi.org/10.1002/palo.20046

Aguiar, A.L., Cirano, M., Pereira, J., Marta-Almeida, M., 2014. Upwelling processes along a western boundary current in the Abrolhos-Campos region of Brazil. Cont. Shelf Res. 85, 42–59. https://doi.org/10.1016/j.csr.2014.04.013

Ahn, J., Brook, E.J., 2008. Atmospheric CO2 and Climate on Millennial Time Scales During the Last Glacial Period. Science (80-.). 322, 83–86.

Bard, E., Rickaby, R.E.M., 2009. Migration of the subtropical front as a modulator of glacial climate. Nature 460, 380–383. https://doi.org/10.1038/nature08189

Barker, S., Diz, P., 2014. Timing of the descent into the last Ice Age determined by the bipolar seesaw. Paleoceanography 29, 489–507. https://doi.org/10.1002/2014PA002623

Barker, S., Greaves, M., Elderfield, H., 2003. A study of cleaning procedures used for foraminiferal Mg/Ca paleothermometry. Geochemistry, Geophys. Geosystems 4, 1–20. https://doi.org/10.1029/2003GC000559

Barnola, J.M., Raynaud, D., Korotkevicht, Y.S., Lorius, C., 1987. Vostok Icecore CO2 changes over last 160,000 years. Nat. Geosci. 329, 408.

Bazin, L., Landais, A., Lemieux-Dudon, B., Toyé Mahamadou Kele, H., Veres, D., Parrenin, F., Martinerie, P., Ritz, C., Capron, E., Lipenkov, V., Loutre, M.F., Raynaud, D., Vinther, B., Svensson, A., Rasmussen, S.O., Severi, M., Blunier, T., Leuenberger, M., Fischer, H., Masson-Delmotte, V., Chappellaz, J., Wolff, E., 2013. An optimized multi-proxy, multi-site Antarctic ice and gas orbital chronology (AICC2012): 120-800 ka. Clim. Past 9, 1715–1731. https://doi.org/10.5194/cp-9-1715-2013

Bereiter, B., Eggleston, S., Schmitt, J., Nehrbass-Ahles, C., Stocker, T.F., Fischer, H., Kipfstuhl, S., Chappellaz, J., 2015. Revision of the EPICA Dome C CO2 record from 800 to 600-kyr before present. Geophys. Res. Lett. 42, 542–549. https://doi.org/10.1002/2014GL061957

Berger, A., Loutre, M.F., 1991. Insolation values for the climate of the last 10 million years. Quat. Sci. Rev. 10, 297–317. https://doi.org/10.1016/0277-3791(91)90033-Q

Berger, A., Loutre, M.F., Yin, Q., 2010. Total irradiation during any time interval of the year using elliptic integrals. Quat. Sci. Rev. 29, 1968–1982. https://doi.org/10.1016/j.quascirev.2010.05.007

Blaauw, M., Christeny, J.A., 2011. Flexible paleoclimate age-depth models using an autoregressive gamma process. Bayesian Anal. 6, 457–474. https://doi.org/10.1214/11-BA618

Blunier, T., Brook, E.J., Science, S., Series, N., Jan, N., 2001. Timing of of Millennial-Scale Millennial-Scale Climate Climate Change Change in in Antarctica and Greenland Greenland During During the the Last 291, 109–112.

Broccoli, A.J., 2000. Tropical cooling at the last glacial maximum: An atmosphere-mixed layer ocean model simulation. J. Clim. 13, 951–976. https://doi.org/10.1175/1520-0442(2000)013<0951:TCATLG>2.0.CO;2

Brook, E.J., Buizert, C., 2018. Antarctic and global climate history viewed from ice cores. Nature 558, 200–208. https://doi.org/10.1038/s41586-018-0172-5

Buizert, C., Adrian, B., Ahn, J., Albert, M., Alley, R.B., Baggenstos, D., Bauska, T.K., Bay, R.C., Bencivengo, B.B., Bentley, C.R., Brook, E.J., Chellman, N.J., Clow, G.D., Cole-Dai, J., Conway, H., Cravens, E., Cuffey, K.M., Dunbar, N.W., Edwards, J.S., Fegyveresi, J.M., Ferris, D.G., Fitzpatrick, J.J., Fudge, T.J., Gibson, C.J., Gkinis, V., Goetz, J.J., Gregory, S., Hargreaves, G.M., Iverson, N., Johnson, J.A., Jones, T.R., Kalk, M.L., Kippenhan, M.J., Koffman, B.G., Kreutz, K., Kuhl, T.W., Lebar, D.A., Lee, J.E., Marcott, S.A., Markle, B.R., Maselli, O.J., McConnell, J.R., McGwire, K.C., Mitchell, L.E., Mortensen, N.B., Neff, P.D., Nishiizumi, K., Nunn, R.M., Orsi, A.J., Pasteris, D.R., Pedro, J.B., Pettit, E.C., Price, P.B., Priscu, J.C., Rhodes, R.H., Rosen, J.L., Schauer, A.J., Schoenemann, S.W., Sendelbach, P.J., Severinghaus, J.P., Shturmakov, A.J., Sigl, M., Slawny, K.R., Souney, J.M., Sowers, T.A., Spencer, M.K., Steig, E.J., Taylor, K.C., Twickler, M.S., Vaughn, B.H., Voigt, D.E., Waddington, E.D., Welten, K.C., Wendricks, A.W., White, J.W.C., Winstrup, M., Wong, G.J., Woodruff, T.E., 2015. Precise interpolar phasing of abrupt climate change during the last ice age. Nature 520, 661–665. https://doi.org/10.1038/nature14401

Cortijo, E., Lehman, S., Keigwin, L., Chapman, M., Paillard, D., Labeyrie, L., 1999. Changes in meridional temperature and salinity gradients in the North Atlantic Ocean (30°-72°N) during the last interglacial period. Paleoceanography 14, 23–33. https://doi.org/10.1029/1998PA900004

Crivellari, S., Chiessi, C.M., Kuhnert, H., Häggi, C., Mollenhauer, G., Hefter, J., Portilho-Ramos, R., Schefuß, E., Mulitza, S., 2019. Thermal response of the western tropical Atlantic to slowdown of the Atlantic Meridional Overturning Circulation. Earth Planet. Sci. Lett. 519, 120–129. https://doi.org/10.1016/j.epsl.2019.05.006

Crowley, T.J., 1992. NORTH ATLANTIC DEEP WATER COOLS THE SOUTHERN HEMISPHE. Paleoceanography 7, 489–497.

Curry, W.B., Lohmann, G.P., 1986. Late Quaternary carbonate sedimentation at the Sierra Leone Rise (eastern equatorial Atlantic Ocean). Mar. Geol. 70, 223–250. https://doi.org/10.1016/0025-3227(86)90004-6

Deaney, E.L., Barker, S., Van De Flierdt, T., 2017. Timing and nature of AMOC recovery across Termination 2 and magnitude of deglacial CO2 change. Nat. Commun. 8, 1–10. https://doi.org/10.1038/ncomms14595

Dittert, N., Henrich, R., 2000. Carbonate dissolution in the South Atlantic Ocean: Evidence from ultrastructure breakdown in Globigerina bulloides. Deep. Res. Part I Oceanogr. Res. Pap. 47, 603–620. https://doi.org/10.1016/S0967-0637(99)00069-2

Dyez, K.A., Ravelo, A.C., 2013. Late Pleistocene tropical Pacific temperature sensitivity to radiative greenhouse gas forcing. Geology 41, 23–26. https://doi.org/10.1130/G33425.1

Fraile, I., Mulitza, S., Schulz, M., 2009. Modeling planktonic foraminiferal seasonality: Implications for sea-surface temperature reconstructions. Mar. Micropaleontol. 72, 1–9. https://doi.org/10.1016/j.marmicro.2009.01.003

Genthon, G., Barnola, J.M., Raynaud, D., Lorius, C., Jouzel, J., Barkov, N.I., Korotkevich, Y.S., Kotlyakov, V.M., 1987. Vostok ice core: Climatic response to CO2 and orbital forcing changes over the last climatic cycle. Nature 329, 414–418. https://doi.org/10.1038/329414a0

Gray, W.R., Evans, D., 2019. Nonthermal Influences on Mg/Ca in Planktonic Foraminifera: A Review of Culture Studies and Application to the Last Glacial Maximum. Paleoceanogr. Paleoclimatology 34, 306–315. https://doi.org/10.1029/2018PA003517

Gray, W.R., Weldeab, S., Lea, D.W., Rosenthal, Y., Gruber, N., Donner, B., Fischer, G., 2018. The effects of temperature, salinity, and the carbonate system on Mg/Ca in Globigerinoides ruber (white): A global sediment trap calibration. Earth Planet. Sci. Lett. 482, 607–620. https://doi.org/10.1016/j.epsl.2017.11.026

Greaves, M., Barker, S., Daunt, C., Elderfield, H., 2005. Accuracy, standardization, and interlaboratory calibration standards for foraminiferal Mg/Ca thermometry. Geochemistry, Geophys. Geosystems 6, 1–9. https://doi.org/10.1029/2004GC000790

Hastenrath, S., Merle, J., 1987. Annual Cycle of Subsurface Thermal Structure in the Tropical

Atlantic Ocean. J. Phys. Oceanogr. 17, 1518–1538.

Heaton, T.J., Köhler, P., Butzin, M., Bard, E., Reimer, R.W., Austin, W.E.N., Bronk Ramsey, C., Grootes, P.M., Hughen, K.A., Kromer, B., Reimer, P.J., Adkins, J., Burke, A., Cook, M.S., Olsen, J., Skinner, L.C., 2020. Marine20 - The Marine Radiocarbon Age Calibration Curve (0-55,000 cal BP). Radiocarbon 62, 779–820. https://doi.org/10.1017/RDC.2020.68

Hodell, D.A., Minth, E.K., Curtis, J.H., McCave, I.N., Hall, I.R., Channell, J.E.T., Xuan, C., 2009. Surface and deep-water hydrography on Gardar Drift (Iceland Basin) during the last interglacial period. Earth Planet. Sci. Lett. 288, 10–19. https://doi.org/10.1016/j.epsl.2009.08.040

Hou, A., Bahr, A., Schmidt, S., Strebl, C., Albuquerque, A.L., Chiessi, C.M., Friedrich, O., 2020. Forcing of western tropical South Atlantic sea surface temperature across three glacial-interglacial cycles. Glob. Planet. Change 188, 103150. https://doi.org/10.1016/j.gloplacha.2020.103150

Johns, W.E., Townsend, T.L., Fratantoni, D.M., Wilson, W.D., 2002. On the Atlantic inflow to the Caribbean Sea. Deep. Res. Part I Oceanogr. Res. Pap. 49, 211–243. https://doi.org/10.1016/S0967-0637(01)00041-3

Jonkers, L., Kučera, M., 2015. Global analysis of seasonality in the shell flux of extant planktonic Foraminifera. Biogeosciences 12, 2207–2226. https://doi.org/10.5194/bg-12-2207-2015

Jouzel, J., Masson-Delmotte, V., Cattani, O., Dreyfus, G., Falourd, S., Hoffmann, G., Minster, B., Nouet, J., Barnola, J.M., Chappellaz, J., Fischer, H., Gallet, J.C., Johnsen, S., Leuenberger, M., Loulergue, L., Luethi, D., Oerter, H., Parrenin, F., Raisbeck, G., Raynaud, D., Schilt, A., Schwander, J., Selmo, E., Souchez, R., Spahni, R., Stauffer, B., Steffensen, J.P., Stenni, B., Stocker, T.F., Tison, J.L., Werner, M., Wolff, E.W., 2007. Orbital and millennial antarctic climate variability over the past 800,000 years. Science (80-.). 317, 793–796. https://doi.org/10.1126/science.1141038

Kara, A.B., Rochford, P.A., Hurlburt, H.E., 2000. An optimal definition for ocean mixed layer depth. J. Geophys. Res. Ocean. 105, 16803–16821. https://doi.org/10.1029/2000jc900072

Kearns, L.E., Searle-Barnes, A., Foster, G.L., Milton, J.A., Standish, C.D., Ezard, T.H.G., 2023. The Influence of Geochemical Variation Among Globigerinoides ruber Individuals on Paleoceanographic Reconstructions. Paleoceanogr. Paleoclimatology 38, 1–20. https://doi.org/10.1029/2022PA004549

Kohfeld, K.E., Chase, Z., 2017. Temporal evolution of mechanisms controlling ocean carbon uptake during the last glacial cycle. Earth Planet. Sci. Lett. 472, 206–215. https://doi.org/10.1016/j.epsl.2017.05.015

Kucera, M., 2007. Chapter Six Planktonic Foraminifera as Tracers of Past Oceanic Environments. Dev. Mar. Geol. 1, 213–262. https://doi.org/10.1016/S1572-5480(07)01011-1

Lea, D.W., 2004. The 100 000-yr cycle in tropical SST, greenhouse forcing, and climate sensitivity. J. Clim. 17, 2170–2179. https://doi.org/10.1175/1520-0442(2004)017<2170:TYCITS>2.0.CO;2

Lee, K., Tong, L.T., Millero, F.J., Sabine, C.L., Dickson, A.G., Goyet, C., Park, G.H., Wanninkhof, R., Feely, R.A., Key, R.M., 2006. Global relationships of total alkalinity with salinity and temperature in surface waters of the world’s oceans. Geophys. Res. Lett. 33, 1–5. https://doi.org/10.1029/2006GL027207

Lessa, D., Morard, R., Jonkers, L., M. Venancio, I., Reuter, R., Baumeister, A., Luiza Albuquerque, A., Kucera, M., 2020. Distribution of planktonic foraminifera in the subtropical South Atlantic: Depth hierarchy of controlling factors. Biogeosciences 17, 4313–4342. https://doi.org/10.5194/bg-17-4313-2020

Lessa, D.V.O., Santos, T.P., Venancio, I.M., Albuquerque, A.L.S., 2017. Offshore expansion of the Brazilian coastal upwelling zones during Marine Isotope Stage 5. Glob. Planet. Change 158, 13–20. https://doi.org/10.1016/j.gloplacha.2017.09.006

Lessa, D.V.O., Santos, T.P., Venancio, I.M., Santarosa, A.C.A., dos Santos Junior, E.C., Toledo, F.A.L., Costa, K.B., Albuquerque, A.L.S., 2019. Eccentricity-induced expansions of Brazilian coastal upwelling zones. Glob. Planet. Change 179, 33–42. https://doi.org/10.1016/j.gloplacha.2019.05.002

Lisiecki, L.E., 2014. Atlantic overturning responses to obliquity and precession over the last 3 Myr. Paleoceanography 29, 71–86. https://doi.org/10.1002/2013PA002505

Lisiecki, L.E., Raymo, M.E., 2005. A Pliocene-Pleistocene stack of 57 globally distributed benthic D 18 O records 20, 1–17. https://doi.org/10.1029/2004PA001071

Lisiecki, L.E., Raymo, M.E., Curry, W.B., 2008. Atlantic overturning responses to Late Pleistocene climate forcings. Nature 456, 85–88. https://doi.org/10.1038/nature07425

Liu, Z., Zhu, J., Rosenthal, Y., Zhang, X., Otto-Bliesner, B.L., Timmermann, A., Smith, R.S., Lohmann, G., Zheng, W., Timm, O.E., 2014. The Holocene temperature conundrum. Proc. Natl. Acad. Sci. U. S. A. 111. https://doi.org/10.1073/pnas.1407229111

Locarnini, R.A., Mishonov, A. V., Baranova, O.K., Boyer, T.P., Zweng, M.M., Garcia, H.E., Reagan, J.R., Seidov, D., Weathers, K.W., Paver, C.R., Smolyar, I. V., 2019. World Ocean Atlas 2018, Volume 1: Temperature. A. Mishonov, Technical Editor. NOAA Atlas NESDIS 81, 52.

Loulergue, L., Schilt, A., Spahni, R., Masson-Delmotte, V., Blunier, T., Lemieux, B., Barnola, J.M., Raynaud, D., Stocker, T.F., Chappellaz, J., 2008. Orbital and millennial-scale features of atmospheric CH4 over the past 800,000 years. Nature 453, 383–386. https://doi.org/10.1038/nature06950

Loutre, M.F., Paillard, D., Vimeux, F., Cortijo, E., 2004. Does mean annual insolation have the potential to change the climate? Earth Planet. Sci. Lett. 221, 1–14. https://doi.org/10.1016/S0012-821X(04)00108-6

Lumpkin, R., Speer, K., 2007. Global ocean meridional overturning. J. Phys. Oceanogr. 37, 2550–2562. https://doi.org/10.1175/JPO3130.1

Lüthi, D., Le Floch, M., Bereiter, B., Blunier, T., Barnola, J.M., Siegenthaler, U., Raynaud, D., Jouzel, J., Fischer, H., Kawamura, K., Stocker, T.F., 2008. High-resolution carbon dioxide concentration record 650,000-800,000 years before present. Nature 453, 379–382. https://doi.org/10.1038/nature06949

Marshall, J., Donohoe, A., Ferreira, D., McGee, D., 2014. The ocean's role in setting the mean position of the Inter-Tropical Convergence Zone. Clim. Dyn. 42, 1967–1979. https://doi.org/10.1007/s00382-013-1767-z

Martínez-garcía, A., Sigman, D.M., Ren, H., Anderson, R.F., Straub, M., Hodell, D.A., Jaccard, S.L., Eglinton, T.I., Haug, G.H., 2014. Iron Fertilization of the Subantarctic Ocean During the Last Ice Age 343, 1347–1350.

McIntyre, A., Ruddiman, W.F., Karlin, K., Mix, A.C., 1989. Surface water response of the equatorial Atlantic Ocean to orbital forcing. Paleoceanography 4, 19–55. https://doi.org/10.1029/PA004i001p00019

Members, E.C., 2006. One-to-one coupling of glacial climate variability in Greenland and Antarctic. Nature 444, 195–198.

Mix, A.C., Fairbanks, G., 1985. North Atlantic surface-ocean control of Pleistocene deep-ocean circulation. Earth Planet. Sci. Lett. 73, 231–243.

Mix, A.C., Ruddiman, W.F., McIntyre, A., 1986. Late Quaternary paleoceanography of the Tropical Atlantic, 1: Spatial variability of annual mean sea-surface temperatures, 0-20,000 years B.P. Paleoceanography 1, 43–66. https://doi.org/10.1029/PA001i001p00043

Muglia, J., Schmittner, A., 2021. Carbon isotope constraints on glacial Atlantic meridional overturning: Strength vs depth. Quat. Sci. Rev. 257, 106844. https://doi.org/10.1016/j.quascirev.2021.106844

Nascimento, R.A., Santos, T.P., Venancio, I.M., Chiessi, C.M., Ballalai, J.M., Kuhnert, H., Govin, A., Portilho-Ramos, R.C., Lessa, D., Dias, B.B., Pinho, T.M.L., Crivellari, S., Mulitza, S., Albuquerque, A.L.S., 2021a. Origin of δ13C minimum events in thermocline and intermediate waters of the western South Atlantic. Quat. Sci. Rev. 272, 107224. https://doi.org/10.1016/j.quascirev.2021.107224

Nascimento, R.A., Shimizu, M.H., Venancio, I.M., Chiessi, C.M., Kuhnert, H., Johnstone, H., Govin, A., Lessa, D., Ballalai, J.M., Piacsek, P., Mulitza, S., Albuquerque, A.L.S., 2022. Warmer western tropical South Atlantic during the Last Interglacial relative to the current interglacial period. Glob. Planet. Change 215, 103889. https://doi.org/10.1016/j.gloplacha.2022.103889

Nascimento, R.A., Venancio, I.M., Chiessi, C.M., Ballalai, J.M., Kuhnert, H., Johnstone, H., Santos, T.P., Prange, M., Govin, A., Crivellari, S., Mulitza, S., Albuquerque, A.L.S., 2021b. Tropical Atlantic stratification response to late Quaternary precessional forcing. Earth Planet. Sci. Lett. 568, 117030. https://doi.org/10.1016/j.epsl.2021.117030

Nürnberg, D., Müller, A., Schneider, R.R., 2000. Paleo-sea surface temperature calculations in the equatorial east Atlantic from Mg/Ca ratios in planktic foraminifera: A comparison to sea surface temperature estimates from U37K′, oxygen isotopes, and foraminiferal transfer function. Paleoceanography 15, 124–134. https://doi.org/10.1029/1999PA000370

Nürnberg, D., Ziegler, M., Karas, C., Tiedemann, R., Schmidt, M.W., 2008. Interacting Loop Current variability and Mississippi River discharge over the past 400 kyr. Earth Planet. Sci. Lett. 272, 278–289. https://doi.org/10.1016/j.epsl.2008.04.051

Pahnke, K., Sachs, J.P., 2006. Sea surface temperatures of southern midlatitudes 0-160 kyr B.P. Paleoceanography 21, 1–17. https://doi.org/10.1029/2005PA001191

Pedro, J.B., Jochum, M., Buizert, C., He, F., Barker, S., Rasmussen, S.O., 2018. Beyond the bipolar seesaw: Toward a process understanding of interhemispheric coupling. Quat. Sci. Rev. 192, 27–46. https://doi.org/10.1016/j.quascirev.2018.05.005

Pinho, T.M.L., Chiessi, C.M., Portilho-Ramos, R.C., Campos, M.C., Crivellari, S., Nascimento, R.A., Albuquerque, A.L.S., Bahr, A., Mulitza, S., 2021. Meridional changes in the South

Atlantic Subtropical Gyre during Heinrich Stadials. Sci. Rep. 11, 1–10. https://doi.org/10.1038/s41598-021-88817-0

Pöppelmeier, F., Jeltsch-Thömmes, A., Lippold, J., Joos, F., Stocker, T.F., 2023. Multi-proxy constraints on Atlantic circulation dynamics since the last ice age. Nat. Geosci. 16. https://doi.org/10.1038/s41561-023-01140-3

Raymo, M.E., Ruddiman, W.F., Shackleton, N.J., Oppo, D.W., 1990. Evolution of Atlantic-Pacific δ13C gradients over the last 2.5 m.y. Earth Planet. Sci. Lett. 97, 353–368. https://doi.org/10.1016/0012-821X(90)90051-X

Rayner, N.A., Parker, D.E., Horton, E.B., Folland, C.K., Alexander, L. V., Rowell, D.P., Kent, E.C., Kaplan, A., 2003. Global analyses of sea surface temperature, sea ice, and night marine air temperature since the late nineteenth century. J. Geophys. Res. Atmos. 108. https://doi.org/10.1029/2002jd002670

Rebotim, A., Voelker, A.H.L., Jonkers, L., Waniek, J.J., Meggers, H., Schiebel, R., Fraile, I., Schulz, M., Kucera, M., 2017. Factors controlling the depth habitat of planktonic foraminifera in the subtropical eastern North Atlantic. Biogeosciences 14, 827–859. https://doi.org/10.5194/bg-14-827-2017

Rodrigues, R.R., Rothstein, L.M., Wimbush, M., 2007. Seasonal variability of the South Equatorial Current bifurcation in the Atlantic Ocean: A numerical study. J. Phys. Oceanogr. 37, 16–30. https://doi.org/10.1175/JPO2983.1

Rohling, E.J., Medina-Elizalde, M., Shepherd, J.G., Siddall, M., Stanford, J.D., 2012. Sea surface and high-latitude temperature sensitivity to radiative forcing of climate over several glacial cycles. J. Clim. 25, 1635–1656. https://doi.org/10.1175/2011JCLI4078.1

Rühlemann, C., Mulitza, S., Muller, P., Wefer, G., Zahn, R., 1999. WarmingofthetropicalAtlanticOcean and slowdown of thermohaline circulation during the last deglaciation. Nature 402, 511–514.

Santos, T.P., Lessa, D.O., Venancio, I.M., Chiessi, C.M., Mulitza, S., Kuhnert, H., Govin, A., Machado, T., Costa, K.B., Toledo, F., Dias, B.B., Luiza, A., Albuquerque, S., 2017. Prolonged warming of the Brazil Current precedes deglaciations. Earth Planet. Sci. Lett. 463, 1–12. https://doi.org/10.1016/j.epsl.2017.01.014

Santos, T.P., Shimizu, M.H., Nascimento, R.A., Venancio, I.M., Campos, M.C., Portilho-Ramos, R.C., Ballalai, J.M., Lessa, D.O., Crivellari, S., Nagai, R.H., Chiessi, C.M., Kuhnert, H., Bahr, A., Albuquerque, A.L.S., 2022. A data-model perspective on the Brazilian margin surface warming from the Last Glacial Maximum to the Holocene. Quat. Sci. Rev. 286. https://doi.org/10.1016/j.quascirev.2022.107557

Schaefer, J.M., Putnam, A.E., Denton, G.H., Kaplan, M.R., Birkel, S., Doughty, A.M., Kelley, S., Barrell, D.J.A., Finkel, R.C., Winckler, G., Anderson, R.F., Ninneman, U.S., Barker, S., Schwartz, R., Andersen, B.G., Schluechter, C., 2015. The Southern Glacial Maximum 65,000 years ago and its Unfinished Termination. Quat. Sci. Rev. 114, 52–60. https://doi.org/10.1016/j.quascirev.2015.02.009

Schmid, C., Schäfer, H., Podestá, G., Zenk, W., 1995. The Vitória eddy and its relation to the Brazil Current. J. Phys. Oceanogr. 25, 2532–2546.

Schmidt, M.W., Spero, H.J., Lea, D.W., 2004. Links between salinity variation in the Caribbean and North Atlantic thermohaline circulation. Nature 428, 160–163. https://doi.org/10.1038/nature02346

Schmidt, M.W., Spero, H.J., Vautravers, M.J., 2006. Western Caribbean sea surface temperatures during the late Quaternary. Geochemistry, Geophys. Geosystems 7. https://doi.org/10.1029/2005GC000957

Schmuker, B., Schiebel, R., 2002. Planktic foraminifers and hydrography of the eastern and northern Caribbean Sea. Mar. Micropaleontol. 46, 387–403. https://doi.org/10.1016/S0377-8398(02)00082-8

Schneider, T., Bischoff, T., Haug, G.H., 2014. Migrations and dynamics of the intertropical convergence zone. Nature 513, 45–53. https://doi.org/10.1038/nature13636

Shakun, J.D., Clark, P.U., He, F., Marcott, S.A., Mix, A.C., Liu, Z., Otto-bliesner, B., Schmittner, A., Bard, E., 2012. Global warming preceded by increasing carbon dioxide concentrations during the last deglaciation. Nature 484, 49–54. https://doi.org/10.1038/nature10915

Spratt, R.M., Lisiecki, L.E., 2016. A Late Pleistocene sea level stack. Clim. Past 12, 1079–1092. https://doi.org/10.5194/cp-12-1079-2016

Srokosz, M., Baringer, M., Bryden, H., Cunningham, S., Delworth, T., Lozier, S., Marotzke, J., Sutton, R., 2012. Past, present, and future changes in the atlantic meridional overturning circulation. Bull. Am. Meteorol. Soc. 93, 1663–1676. https://doi.org/10.1175/BAMS-D-11-00151.1

Steinke, S., Chiu, H.Y., Yu, P. Sen, Shen, C.C., Löwemark, L., Mii, H.S., Chen, M. Te, 2005. Mg/Ca ratios of two Globigerinoides ruber (white) morphotypes: Implications for reconstructing past tropical/subtropical surface water conditions. Geochemistry, Geophys. Geosystems 6, 1–12. https://doi.org/10.1029/2005GC000926

Stocker, T.F., Johnsen, S.J., 2003. A minimum thermodynamic model for the bipolar seesaw. Paleoceanography 18, 1–19. https://doi.org/10.1029/2003PA000920

Stramma, L., England, M., 1999. On the water masses and mean circulation of the South Atlantic Ocean. J. Geophys. Res. 104.

Tachikawa, K., Timmermann, A., Vidal, L., Sonzogni, C., Timm, O.E., 2014. CO2 radiative forcing and Intertropical Convergence Zone influences on western Pacific warm pool climate over the past 400ka. Quat. Sci. Rev. 86, 24–34. https://doi.org/10.1016/j.quascirev.2013.12.018

Takahashi, T., Sutherland, S.C., Wanninkhof, R., Sweeney, C., Feely, R.A., Chipman, D.W., Hales, B., Friederich, G., Chavez, F., Sabine, C., Watson, A., Bakker, D.C.E., Schuster, U., Metzl, N., Yoshikawa-Inoue, H., Ishii, M., Midorikawa, T., Nojiri, Y., Körtzinger, A., Steinhoff, T., Hoppema, M., Olafsson, J., Arnarson, T.S., Tilbrook, B., Johannessen, T., Olsen, A., Bellerby, R., Wong, C.S., Delille, B., Bates, N.R., de Baar, H.J.W., 2009. Climatological mean and decadal change in surface ocean pCO_2, and net sea-air CO_2 flux over the global oceans. Deep. Res. Part II Top. Stud. Oceanogr. 56, 554–577. https://doi.org/10.1016/j.dsr2.2008.12.009

Thornalley, D.J.R., Barker, S., Becker, J., Hall, I.R., Knorr, G., 2013. Abrupt changes in deep Atlantic circulation during the transition to full glacial conditions. Paleoceanography 28, 253–262. https://doi.org/10.1002/palo.20025

Timmermann, A., Lorenz, S.J., An, S.I., Clement, A., Xie, S.P., 2007. The effect of orbital forcing on the mean climate and variability of the tropical Pacific. J. Clim. 20, 4147–4159. https://doi.org/10.1175/JCLI4240.1

Toggweiler, J.R., Russell, J.L., Carson, S.R., 2006. Midlatitude westerlies , atmospheric CO_2 , and climate change during the ice ages. Paleoceanography 21, 1–15. https://doi.org/10.1029/2005PA001154

Vellinga, M., Wu, P., 2004. Low-latitude freshwater influence on centennial variability of the Atlantic thermohaline circulation. J. Clim. 17, 4498–4511. https://doi.org/10.1175/3219.1

Venancio, I.M., Belem, A.L., Santos, T.P., Lessa, D.O., Albuquerque, A.L.S., Mulitza, S., Schulz, M., Kucera, M., 2017. Calcification depths of planktonic foraminifera from the southwestern Atlantic derived from oxygen isotope analyses of sediment trap material. Mar. Micropaleontol. 136, 37–50. https://doi.org/10.1016/j.marmicro.2017.08.006

Venancio, I.M., Franco, D., Belem, A.L., Mulitza, S., Siccha, M., Albuquerque, A.L.S., Schulz, M., Kucera, M., 2016. Planktonic foraminifera shell fluxes from a weekly resolved sediment trap record in the southwestern Atlantic: Evidence for synchronized reproduction. Mar. Micropaleontol. 125, 25–35. https://doi.org/10.1016/j.marmicro.2016.03.003

Venancio, I.M., Shimizu, M.H., Santos, T.P., Lessa, D.O., Dias, B.B., Chiessi, C.M., Mulitza, S., Kuhnert, H., Tiedemann, R., Vahlenkamp, M., Bickert, T., Belem, A.L., Sampaio, G., Albuquerque, A.L.S., Nobre, C., 2020. Ocean-atmosphere interactions over the western South Atlantic during Heinrich stadials. Glob. Planet. Change 195, 103352.

https://doi.org/10.1016/j.gloplacha.2020.103352

Veres, D., Bazin, L., Landais, A., Toyé Mahamadou Kele, H., Lemieux-Dudon, B., Parrenin, F., Martinerie, P., Blayo, E., Blunier, T., Capron, E., Chappellaz, J., Rasmussen, S.O., Severi, M., Svensson, A., Vinther, B., Wolff, E.W., 2013. The Antarctic ice core chronology (AICC2012): An optimized multi-parameter and multi-site dating approach for the last 120 thousand years. Clim. Past 9, 1733–1748. https://doi.org/10.5194/cp-9-1733-2013

Weldeab, S., Schneider, R.R., Kölling, M., 2006. Deglacial sea surface temperature and salinity increase in the western tropical Atlantic in synchrony with high latitude climate instabilities. Earth Planet. Sci. Lett. 241, 699–706. https://doi.org/10.1016/j.epsl.2005.11.012

Yang, J., 1999. A linkage between decadal climate variations in the labrador sea and the tropical atlantic ocean. Geophys. Res. Lett. 26, 1023–1026. https://doi.org/10.1029/1999GL900181

Žarić, S., Donner, B., Fischer, G., Mulitza, S., Wefer, G., 2005. Sensitivity of planktic foraminifera to sea surface temperature and export production as derived from sediment trap data. Mar. Micropaleontol. 55, 75–105. https://doi.org/10.1016/j.marmicro.2005.01.002

Zhang, D., Msadek, R., McPhaden, M.J., Delworth, T., 2011. Multidecadal variability of the North Brazil Current and its connection to the Atlantic meridional overturning circulation. J. Geophys. Res. 116, 1–9. https://doi.org/10.1029/2010jc006812

Ziegler, M., Nürnberg, D., Karas, C., Tiedemann, R., Lourens, L.J., 2008. Persistent summer expansion of the Atlantic Warm Pool during glacial abrupt cold events. Nat. Geosci. 1, 601–605. https://doi.org/10.1038/ngeo277

Zweng, M.M., Reagan, J.R., Seidov, D., Boyer, T.P., Antonov, J.I., Locarnini, R.A., Garcia, H.E., Mishonov, A. V., Baranova, O.K., Weathers, K.W., Paver, C.R., Smolyar, I. V., 2019. World Ocean Atlas 2018 Volume 2: Salinity. NOAA Atlas NESDIS 82, 50pp.